REPUBLIC OF TURKEY

YILDIZ TECHNICAL UNIVERSITY

GRADUATE SCHOOL OF NATURAL AND APPLIED SCIENCES

DEVELOPMENT OF BORON CARBIDE - CALCIUM HEXABORIDE CERAMIC COMPOSITES

Yasin Bozkurt YILMAZ

MASTER OF SCIENCE THESIS

Department of Metallurgical and Materials Engineering

Program of Materials Engineering

Advisor

Asst. Prof. Dr. Buğra ÇİÇEK

July, 2020

REPUBLIC OF TURKEY

YILDIZ TECHNICAL UNIVERSITY

GRADUATE SCHOOL OF NATURAL AND APPLIED SCIENCES

DEVELOPMENT OF BORON CARBIDE - CALCIUM HEXABORIDE CERAMIC COMPOSITES

A thesis submitted by Yasin Bozkurt YILMAZ in partial fulfillment of the requirements for the degree of MASTER OF SCIENCE is approved by the committee on 21.07.2020 in Department of Metallurgical and Materials Engineering, Materials Science and Engineering Program.

Asst. Prof. Dr. Buğra ÇİÇEK

Yıldız Technical University

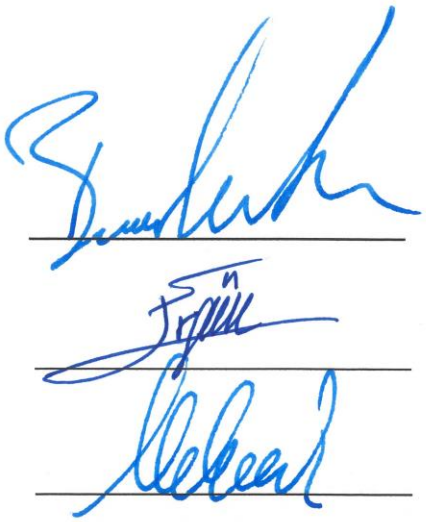
Advisor

Approved By the Examining Committee

Asst. Prof. Dr. Buğra ÇİÇEK, Advisor
Yıldız Technical University

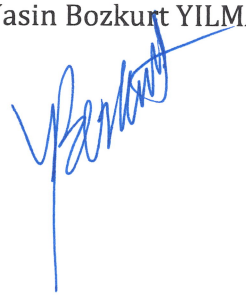
Assoc. Prof. Dr. Ergün KELEŞOĞLU, Member
Yıldız Technical University

Prof. Dr. Mehmet SOMER, Member
Koç University



I hereby declare that I have obtained the required legal permissions during data collection and exploitation procedures, that I have made the in-text citations and cited the references properly, that I haven't falsified and/or fabricated research data and results of the study and that I have abided by the principles of the scientific research and ethics during my Thesis Study under the title of Development of Boron Carbide - Calcium Hexaboride Ceramic Composites supervised by my supervisor, Assist. Prof. Buğra ÇİÇEK. In the case of a discovery of false statement, I am to acknowledge any legal consequence.

Yasin Bozkurt YILMAZ



Dedicated to my family

and thin rose of my thoughts..

ACKNOWLEDGEMENTS

First of all, I would like to express my deepest appreciation to my advisor Asst. Prof. Dr. Buğra ÇİÇEK for sharing his deep knowledge with me and for giving me the freedom and confidence to develop my ideas. Without his guidance and persistent help, this thesis would not have been possible.

I would like to thank Gizem Seramik Frit and Glazur San. ve Tic. A.S. for providing the necessary support in my work. I am also grateful to researchers in Gizemfrit R&D Center and Cicek's Advanced Ceramics Research Group for their help through my experimental and characterization work.

I would like to give my special thanks to my sister Nisa Asena, my father Emin and my mother Halise. They made possible everything I wanted, all my life long. Without their support, patience and love, I could not have achieved all of this.

Finally, I would like to sincerely thank Dr. Tuğçe Nur KARAARSLAN, for her patience and support. I have always been inspired by her hardworking and discipline.

Bursa, 2020

Yasin Bozkurt YILMAZ

TABLE OF CONTENTS

LIST OF SYMBOLS **IX**

LIST OF ABBREVIATIONS **XI**

LIST OF FIGURES **XIII**

LIST OF TABLES **XV**

ABSTRACT **XVI**

ÖZET **XIX**

1 INTRODUCTION **1**

1.1 Literature Review 1

1.2 Objective of the Thesis 3

1.3 Hypothesis 3

2 BORON AND COMPOUNDS **4**

2.1 General Properties of Boron 4

2.1.1 Atomic Structure 5

2.1.2 Physical and Mechanical Properties 6

2.1.3 Chemical Properties 7

2.2 Usage Areas of Boron 7

2.3 Boron Carbide 9

2.3.1 General Properties and Use Areas 9

2.3.2 Synthesis Methods 12

2.4 Calcium Hexaboride 12

2.4.1 General Properties General Properties and Usage Areas 13

2.4.2 Synthesis Methods 15

3 SINTERING AND CERAMIC COMPOSITES 17

3.1 Sintering ... 17

3.1.1 Solid State Sintering ... 18

3.1.2 Liquid Phase Sintering ... 20

3.1.3 Reaction Sintering ... 21

3.1.4 Pressure Assisted Sintering ... 21

3.2 Ceramic Composites ... 24

3.2.1 Sintering Additives of Boron Carbide ... 25

3.2.2 B_4C-CaB_6 ... 27

4 EXPERIMENTAL SECTION 29

4.1 Materials ... 29

4.2 Preparation of Samples ... 29

4.3 Spark Plasma Sintering of Samples ... 30

5 CHARACTERIZATION STUDIES 33

5.1 Characterization of Raw Materials ... 33

5.2 Sintering Ability ... 33

5.3 Density and Open Porosity ... 33

5.4 XRD Phase Analysis ... 34

5.5 Microstructural Analysis ... 34

5.6 Mechanical Tests ... 34

6 RESULTS AND DISCUSSIONS 36

6.1 Characterization Results of Raw Materials ... 36

6.2 Sintering Behaviour of B_4C at Different Temperature ... 38

6.3 Sintering Behaviour of CaB_6 ... 40

6.4 Effect of CaB_6 Ratio on Sintering Behaviour of B_4C ... 41

6.5 Density and Open Porosity ... 44

6.6 Phase Analysis 45
6.7 Microstructural Analysis 46
6.8 Hardness and Fracture Toughness 56
6.9 Conclusion and Recommendation 58
REFERENCES **61**
PUBLICATIONS FROM THE THESIS **70**

LIST OF SYMBOLS

%	percentage
~	tilde
°	degree
°C	celcius
µm	micrometer
µm	micrometer
Å	ångström
b	barn
cm	centimeter
cm^3	cubic centimeter
E	elastic modulus
g	gram
g/cm^3	density
GPa	gigapascal
h	hour
J	joule
K	kelvin
kA	kiloampere
kg	kilogram
kPa	kilopascal
kV	kilovolt
mg	miligram
mm	milimeter

mm^2	square milimeter
MPa	megapascal
$MPa.m^{½}$	fracture toughness unit
ms	millisecond
N	Newton
s	second
ß	beta
vol%	volume percentage
W	watt
wt%	mass percentage
α	alpha
ρ	Density

LIST OF ABBREVIATIONS

B	Boron
B_2O_3	Boron Oxide
B_4C	Boron Carbide
bcc	Body Centered Cubic
C	Carbon
Ca	Calcium
CaB_6	Calcium Hexaboride
$CaCO_3$	Calcium Carbonate
CaO	Calcium Oxide
CO	Carbon Monoxide
EDS	Energy-dispersive X-Ray Spectroscopy
fcc	Face Centered Cubic
HIP	Hot Isostatic Press
HP	Hot Press
HV	Vickers Hardness
IPA	Isopropyl Alcohol
K_{IC}	Fracture Toughness
RPM	Revoluations Per Minute
SEM	Scanning Electron Microscopy
SiC	Silicon Carbide
SPS	Spark Plasma Sintering
TiB_2	Titanium Diboride
TiC	Titanium Carbide

XRD	X-Ray Diffraction

LIST OF FIGURES

Figure 2.1 Boron Crystal Structure 6
Figure 2.2 Major End User Industry of Borates 8
Figure 2.3 Boron Products 9
Figure 2.4 Boron – Carbon Phase Diagram 10
Figure 2.5 Crystal Structure of B_4C 11
Figure 2.6 Bonding Structure of CaB_6 13
Figure 2.7 B-Ca Phase Diagram by atomic percent and weight percent of Ca 14
Figure 2.8 Crystal Structure of CaB_6 14
Figure 3.1 Schematic Drawing of Sintering Process 17
Figure 3.2 Mechanism of Diffisuon and Transfer 19
Figure 3.3 Two-Sphere Model 19
Figure 3.4 Schematically Drawing of Liquid Phase Sintering 20
Figure 3.5 Liquid Phase Sintering Mechanism a) contact flattening b) dissolution of small grains c) solid state bonding 21
Figure 3.6 Schematecially Drawing of Reaction Sintering 21
Figure 3.7 Schematic Drawing of Hot Press 22
Figure 3.8 Schematic Drawing of Hot Isostatic Press 23
Figure 3.9 Schematic Drawing of Spark Plasma Sintering 24
Figure 4.1 Schematic Representation of the Mold System Used in SPS 31
Figure 6.1 XRD Patterns of Raw Materials 36
Figure 6.2 SEM Image of Boron Carbide Powder and EDS Mapping Results a) Secondary Image b) EDS Mapping Illustration 37
Figure 6.3 SEM Image of Calcium Hexaboride Powders 38
Figure 6.4 Sintering Curve of B100 Sample at 2050 °C 39
Figure 6.5 Sintering Curve of B100 Sample at 1900 °C 40
Figure 6.6 Sintering Curve of C100 at 1850 °C 41
Figure 6.7 Sintering Curve of BC5 Sample at 1900 °C 42
Figure 6.8 Sintering Curve of BC10 Sample at 1900 °C 42
Figure 6.9 Sintering Curve of BC15 Sample at 1900 °C 43
Figure 6.10 Sintering Curve of BC20 Sample at 1900 °C 44

Figure 6.11 Sintering XRD Patterns of Sintered Samples a) B100 b) BC5 c) BC10 d) BC15 e) BC20 46
Figure 6.12 SEM Image of B100 Sample 47
Figure 6.13 SEM Image and EDS Spots of B100 Sample 48
Figure 6.14 EDS Analysis of B100 Sample 49
Figure 6.15 SEM-Secondary Electron Image of BC5 Sample 50
Figure 6.16 SEM Image and EDS Spots of BC5 Sample 50
Figure 6.17 EDS Analysis of BC5 Sample 51
Figure 6.18 SEM-Back Scattered Electron Image of BC10 Sample (1000x) 52
Figure 6.19 SEM-Back Scattered Electron Image of BC10 Sample (20000x) 53
Figure 6.20 SEM-Back Scattered Electron Image of BC15 Sample (5000x) 54
Figure 6.21 SEM-Back Scattered Electron Image of BC15 Sample (20000x) 55
Figure 6.22 SEM-Back Scattered Electron Image of BC20 Sample (20000x) 55
Figure 6.23 SEM Image and EDS Spots of BC20 Sample 56
Figure 6.24 Effect of CaB6 Ratio on Fracture Toughness and Hardness 57

LIST OF TABLES

Table 2.1 Commercial Deposits of Boron Minerals and Boron Content 4
Table 2.2 Atomic Properties of Boron 5
Table 2.3 Physical and Mechanical Properties of Boron 6
Table 2.4 Chemical Properties of Boron 7
Table 2.5 General Properties of B_4C 11
Table 2.6 General Properties of CaB_6 15
Table 4.1 Sample Designation and Compositions 29
Table 4.2 Homogenisation Parameters 29
Table 4.3 Sintering Parameters 31
Table 6.1 EDS Analysis of Boron Carbide Powders 37
Table 6.2 EDS Analysis of Calcium Hexaboride Powders 38
Table 6.3 Open Porosity and Densities of Samples 45
Table 6.4 EDS Analysis of BC5 Sample 51
Table 6.5 EDS Analysis of BC20 Sample 51

ABSTRACT

Development of Boron Carbide – Calcium Hexaboride Ceramic Composites

Yasin Bozkurt YILMAZ

Department of Metallurgical and Materials Engineering

Master of Science Thesis

Advisor: Asst. Dr. Buğra ÇİÇEK

Boron carbide (B_4C) is the hardest material known after diamond and cubic boron nitride. It has many superior properties such as high temperature resistance, low density and chemical inertness. It is preferred in many fields in industry, from cutting tool inserts to ballistic protective plates. B_4C shows its superior properties in forms with high density. However strong covalent bonds, which are the source of their superior properties, limit sinterability. Sinter additives are used to increase the sinterability of B_4C. The high density of sinter additives eliminates the low density advantage of B_4C. In addition, the mechanical properties of the sinter additives used differ from B_4C, which affects the end product properties negatively.

In this study, the use of calcium hexaboride (CaB_6), whose mechanical and physical properties are similar to B_4C, was investigated as a sinter additive. B_4C-CaB_6 mixtures containing 0%, 5%, 10%, 15%, 20% CaB_6 were prepared. The prepared mixes were sintered under vacuum at 1900 °C and 30 MPa under Spark Plasma Sintering (SPS). Density-open porosity, hardness-toughness values of the samples obtained were measured. Phase transformations were analyzed by XRD method. Microstructures were analyzed by SEM-EDS.

As a result of experimental studies, a decrease in sintering onset temperatures was observed depending on the rate of CaB_6 addition. The addition of 20 wt% CaB_6 resulted in sintering at 1300 °C by lowering the start temperature of sintering by 330 °C compared to monolithic B_4C. The relative density increased with the addition of CaB_6, and the open porosity decreased from 4.54% to 0.05%. Hardness value decreased by 6 points and decreased from HV 29.57 GPa to HV 23.41 GPa. The fracture toughness increased by 0.6 points and rise from 5.71 MPa.m^{½} to 6.31 MPa.m^{½}. As a result of XRD analysis, it was observed that there was no reaction between B_4C and CaB_6 and there was no phase transformation. In microstructure studies with SEM, it was observed that CaB_6 phase was homogeneously distributed in the B_4C matrix.

Keywords: Ceramic matrix composites, sintering aids, sintering additives, advanced ceramics

ÖZET

Bor Karbür – Kalsiyum Hekzaborür Seramik Kompozitler Geliştirilmesi

Yasin Bozkurt YILMAZ

Metalurji ve Malzeme Mühendisliği Bölümü

Yüksek Lisans Tezi

Danışman: Dr. Öğr. Üyesi Buğra ÇİÇEK

Bor karbür (B_4C), elmas ve kübik bor nitrürden sonra bilenen en sert malzemedir. Yüksek sıcaklık dayanımı, düşük yoğunluk ve kimyasal inertlik gibi bir çok üstün özelliğe sahiptir. Endüstride kesici takım uçlarından balistik koruyucu plakalara kadar bir çok alanda tercih edilmektedir. B_4C, sahip olduğu üstün özellikleri yüksek yoğunluğa sahip olduğu formlarda göstermektedir. Fakat üstün özelliklerinin kaynağı olan güçlü kovalent bağları sinterlenebilirliğini kısıtlamaktadır. B_4C'nin sinterlenebilirliğini artırmak için sinter katkıları kullanılmaktadır. Sinter katkılarının yoğunluğunun yüksek olması B_4C'nin sahip olduğu düşük yoğunluk avantajını ortadan kaldırmaktadır. Ayrıca kullanılan sinter katkılarının mekanik özelliklerinin B4C'den farklı olması, son ürün özelliklerini olumsuz etkilemektedir.

Bu çalışmada mekanik ve fiziksel özellikleri B_4C ile benzerlik gösteren kalsiyum hekzaborür'ün (CaB_6) sinter katkısı olarak kullanımı araştırılmıştır. Ağırlıkça 0%, 5%, 10%, 15%, 20% CaB_6 içeren B_4C-CaB_6 karışımları hazırlanmıştır. Hazırlanan karışımlar Spark Plazma Sinterleme (SPS) ile vakum altında 1900 °C ve 30 MPa basınç altında sinterlenmiştir. Elde edilen numunelerin yoğunluk – açık porozite,

sertlik-tokluk ölçümleri yapılmıştır. Faz dönüşümleri XRD yöntemi ile analiz edilmiştir.. Mikroyapılar, SEM-EDS ile incelenmiştir.

Deneysel çalışmalar sonucunda CaB_6 ilavesinin oranına bağlı olarak sinterlenme başlangıç sıcaklıklarında azalış görülmüştür. 20 wt% CaB_6 ilavesi, monolitik B_4C'ye kıyasla sinterlenme başlangıç sıcaklığı 330 °C düşürerek 1300 °C'de sinterlenmeye başlanmasını sağlamıştır. Relatif yoğunluk CaB_6 ilavesi ile artmış, görünür porozite oranı 4,54%'ten 0,05%'e kadar düşmüştür. Sertlik değeri 6 puan azalarak HV 29,57 GPa'dan HV 23,41 GPa'ya gerilemiştir. Kırılma tokluğu ise 0,6 puan artarak 5,71 $MPa.m^{½}$'den 6,31 $MPa.m^{½}$ 'ya yükselmiştir. XRD analizleri sonucunda B_4C ve CaB_6 arasında reaksiyon gerçekleşmediği ve faz dönüşümü olmadığı görülmüştür. SEM ile yapılan mikroyapı incelemelerinde CaB_6 fazının B_4C matrisi içinde homojen dağıldığı gözlemlenmiştir.

Anahtar Kelimeler: Seramik matrisli kompozitler, sinterleme katkıları, ileri teknoloji seramikler

1
INTRODUCTION

1.1 Literature Review

Boron carbide (B_4C) is a covalently bonded compound composed of boron (B) and carbon (C). It is the third hardest material after diamond and cubic boron nitride (c-BN). It has a refractory property due to its high temperature, chemicals, and abrasion resistance. It also has a neutron absorption feature. Due to its high hardness, it is used in many areas of the industry, such as nuclear power plants, melting furnaces, primarily cutting tools and defence industry [1]–[4].

Mechanically compacted B_4C cannot reach full density. Therefore, its mechanical properties are low. B_4C shows its superior features in sintered form. Sintering is a term used in powder metallurgy. The sintering process aims to reduce the porosity of formed porous structures with the help of heat. It is aimed to reach the superior mechanical properties of the raw materials by reducing the powder surface areas, increasing the particle contact. B_4C has low sinterability due to its low ion diffusion mobility and strong covalent bonds. The theoretical pressureless sintering temperature of monolithic B_4C is 2200 °C. Different sintering methods and sintering agents are used to increase sintering ability. The most commonly used sintering method for sintering of B_4C is the pressure-assisted sintering technique. Hot press (HP), hot isostatic press (HIP), and spark plasma sintering (SPS) are the most widely used methods in this technique. Also, sintering ability is increased with metallic and ceramic sinter additives. The most commonly used sinter additives are silicon carbide (SiC), titanium diboride (TiB_2), and titanium carbide (TiC). However, the difference between B_4C and additives properties such as density, thermal expansion, melting point, and hardness makes it difficult to reach the desired mechanical properties [5]–[7].

Calcium Hexaboride (CaB_6), also known as calcium boride is a compound consisting of calcium and boron atoms [8], [9]. It has low density (2,45 g/cm^3), high melting

temperature (2235 °C) and high hardness [10], [11]. It has high electrical conductivity, therefore it used as a cathode in metallurgical processes such as copper refining [12]. It is also used in n-type conductors [13]. CaB_6 used in cutting tool due to its high hardness, surface protection and furnace refractory bricks due to its refractory properties [10], [14], [15]. Its mechanical and physical properties are similar to B_4C. Compared to other sinter additives, they have similar properties, thus reducing the possibility of disadvantages such as thermal strain and high density in B_4C-CaB_6 composites.

There are a limited studies in the literature on B_4C-CaB_6 composites. Galanov et al examined the mechanical properties of B_4C-CaB_6 composites containing different rates (10-20-30-40 vol%) of CaB_6[16]. Prepared composites were sintered with hot press at 2150 °C and 30 MPa pressure. CaB_6 addition effectuate microcracks, causing a decrease in mechanical properties. The addition of 10vol% CaB_6 caused the flexural strength to decrease by 40 MPa to decrease from 420 MPa to 380 MPa. With increasing CaB_6 ratio (30 vol%), flexural strength has reached its former value (420 MPa). Composites containing 20vol% and 40vol% CaB_6 increased 5 MPa in flexural strength and reached 425 MPa. In the hardness measurements performed at 2N load, it was measured that the monolithic B_4C hardness of 34.9 GPa reached 39.5 MPa with 20vol% CaB_6 addition. With the 40vol% addition, it has regressed to its standart sample hardness value. In hardness measurements with 200 N, similar changes were observed in the hardness value with increasing CaB_6 ratio. With the addition of 40vol% CaB_6, the hardness value increased by 9 GPa and reached 25 GPa from 16 GPa. In general, there was no continuous improvement in mechanical properties with increasing CaB_6 ratio. When microstructures were examined, it was seen that CaB_6 accumulated in grain boundaries and prevented B_4C recrystallization of B_4C powders.

In the study by Oiao et al, different rates (5-10-15-20vol%) of CaB_6 were added to the B_4C-10vol% Al_2O_3 composite [17]. Samples were sintered with hot press at 30 MPa and 1900 °C. The CaB_6 addition positively affected the sinterability of B_4C. The addition of 20vol% CaB_6 increased the relative intensity from 92% to 96%. The addition of CaB_6 generally improved hardness. The addition of 15vol% CaB_6

improved the hardness value from 36.5 GPa to 39.5. The difference in thermal expansion coefficient between B_4C and CaB_6 caused microfractures. Microfractures formed in composites containing high amount (20vol%) of CaB_6 caused a decrease in hardness values.

1.2 Objective of the Thesis

The first aim of the study is to increase the sinterability of B_4C at low temperatures (1900 °C) with the addition of CaB_6 and to reach the maximum theoretical density. CaB_6 is a more suitable agent for sintering compared to other sinter additives due to its mechanical and physical properties similar to B_4C.

In order to examine the effect of CaB_6 ratio on sintering behavior and mechanical properties, compositions containing different ratios of CaB_6 were prepared except for the reference sample without additives. Spark plasma sintering method, which is the most suitable production for laboratory scale, was preferred to examine the sintering behavior. Sintering behavior of the SPS furnace with shrinkage graph was examined.

Finally, composites have been characterized and studied to see the effects of CaB_6 additive and additive ratios on microstructure and mechanical properties on phase formation and distribution.

1.3 Hypothesis

B_4C has low sintering ability. CaB_6 has similar properties with B_4C mechanically and physically. With the addition of CaB_6, it is predicted to improve the sintering ability of B_4C, to reach the maximum theoretical density at low temperature (1900 °C) without decrease mechanical properties.

2
BORON AND COMPOUNDS

2.1 General Properties of Boron

Boron is a metalloid located between metal and nonmetals in the 3A group in the periodic table. Its symbol is "B". The atomic number is 5. It has two isotopes with mass numbers 10 and 11 [18]–[20]. The presence rate of B^{10} isotope in nature is 19.1-20.3%, while B^{11} isotope is 79.7-80.9% [21]. Average boron concentration in the earth's crust is 10 mg/kg [22].

Boron is not found in elemental nature due to its high affinity. There are boron in 150 different minerals [23]. Commercially important boron minerals are given in Table 2.1. There is the world's boron reserves of 73% were in Turkey. The largest reserves after Turkey are located in the United States, Russia and China respectively [24].

Table 2.1 Commercial Deposits of Boron Minerals and Boron Content [21], [24], [25]

Minerals Name	Compositions	Boron Content (wt%)
Boracite	$Mg_6B_{14}O_{26}Cl_2$	19.30
Colemanite	$Ca_2B_6O_{11}.5H_2O$	15.78
Datolite	$CaBSiO_4.OH$	6.76
Hydroboracite	$CaMgB_6O_{11}.6H_2O$	15.69
Kernite	$Na_2B_4O_7.4H_2O$	14.90
Priceite	$Ca_4B_{10}O_{19}.7H_2O$	15.48
Proberite	$NaCaB_5O_9.5H_2O$	15.39

Table 2.1 Commercial Deposits of Boron Minerals and Boron Content [21], [24], [25] (Continued)

Sassolite	H_3BO_3	17.48
Szaibelyite	$MgBO_2.H_2O$	12.85
Tincal (borax)	$Na_2B_4O_7.10H_2O$	11.34
Tinkalconite	$Na_2B_4O_7.5H_2O$	15.16
Ulexite	$NaCaB_5O_9.8H_2O$	13.34

There are various allotropes of boron. Amorphous boron is a dark brown powder, crystalline boron is black and has hard form. Amorphous boron reacts more reactive than crystalline boron [26], [27].

2.1.1 Atomic Structure

Electron configuration of boron atom is $1s^2\ 2s^2\ 2p^1$ [21]. The crystal boron unit has 12 boron atoms. They have 3 basic crystal forms [21] (Figure 2.1):

1. Alfa-rhombohedral
2. Thetragonal
3. Beta-rhombohedral

Atomic properties of the boron element are given in Table 2.2.

Table 2.2 Atomic Properties of Boron [28], [29]

Properties	**Values**
Number of electrons	5
Number of protons	5
Number of neutrons	6
Atomic Radius	1.17 Å

Table 2.2 Atomic Properties of Boron [28], [29] (Continued)

Ionic Radius	0.23 Å
Atomic Volume	4.6 cm^3/mol

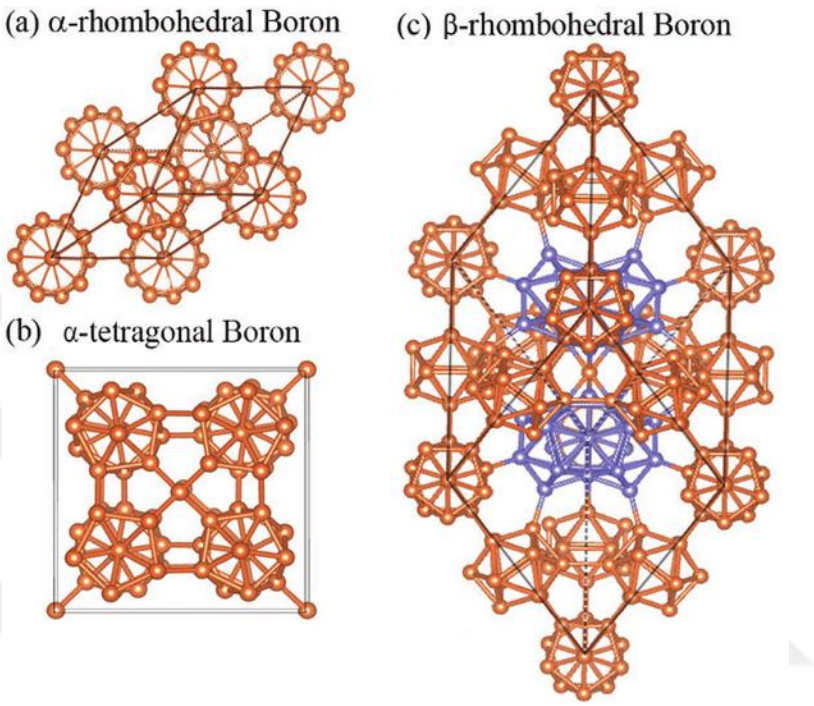


Figure 2.1 Sample Figure Boron crystal structure [30]

2.1.2 Physical and Mechanical Properties

B is solid at room temperature. The melting point is about 2300 °C, although it is variable. The general physical and mechanical properties of the boron element are given in the Table 2.3 [21], [29], [31].

Table 2.3 Physical and Mechanical Properties of Boron [21], [29], [31]

Properties	**Value**
Atomic Mass	93,13 g/mol
Density	2,34 g/cm^3

Table 2.3 Physical and Mechanical Properties of Boron [21], [29], [31] (Continued)

Boiling Point	4002 °C
Melting Point	2300 °C
Hardness	2100-2580 HK (Knopp) 11 (Mohs) 5000 HV (Vickers)
Elastic Modulus	320 GPa

2.1.3 Chemical Properties

Boron is not present elementally in nature. It tends to make compounds due to its high affinity. Chemical properties of boron element are given in the Table 2.4[21], [29], [31].

Table 2.4 Chemical Properties of Boron [21], [29], [31]

Properties	**Values**
Ionization Potential	First: 8.298 Second: 25.154 Third: 37.93
Valance Electron Potential	190 -eV
Fusion Heat	50.2 kJ/mol
Electronegativity	2.04 (pauling)
Electrochemical equivalent	0.1344 (g/A.h)

2.2 Usage Areas of Boron

Boron is used in different sectors such as glass industry, chemistry, textile, agriculture and metallurgy [32] (Figure 2.2). Boron minerals are not suitable for

direct use in end product production. After minerals enrichment, midproducts such as boric acid (H_3BO_3), borax pentahydrate ($Na_2B_4O_7.5H_2O$), anhydrous borax ($Na_2B_4O_7$), sodium perborate ($NaBO_3.4H_2O$) are produced. The midproducts are processed through various processes according to the area of use and the final product is obtained [32], [33] (Figure 2.3).

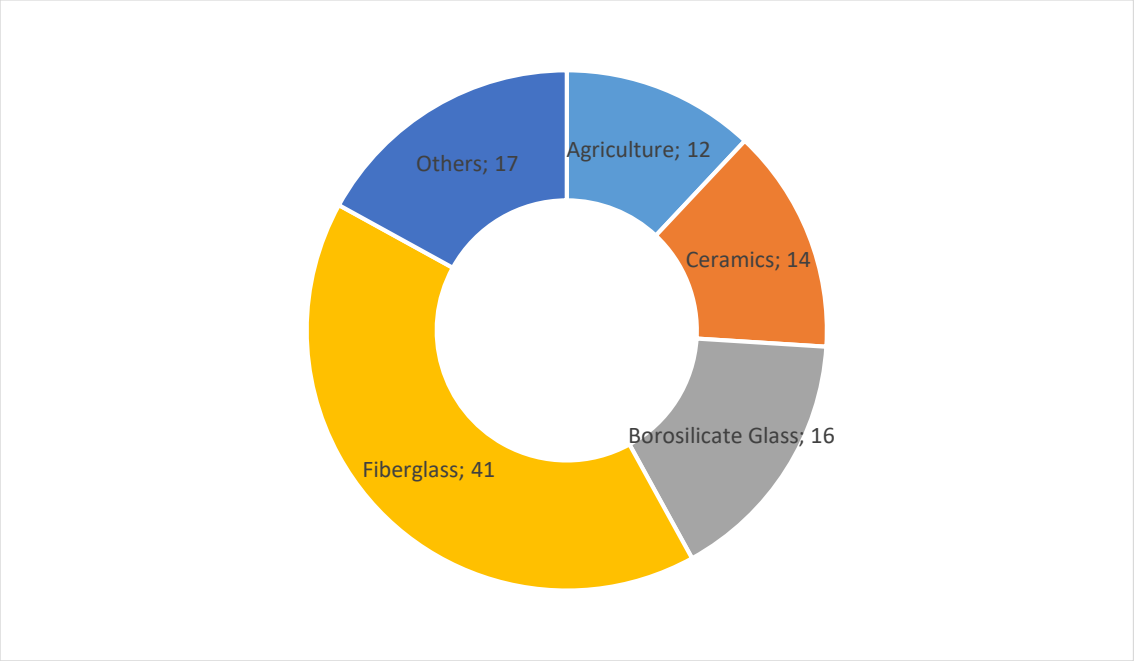


Figure 2.1 Major End User Industry of Borates [32]

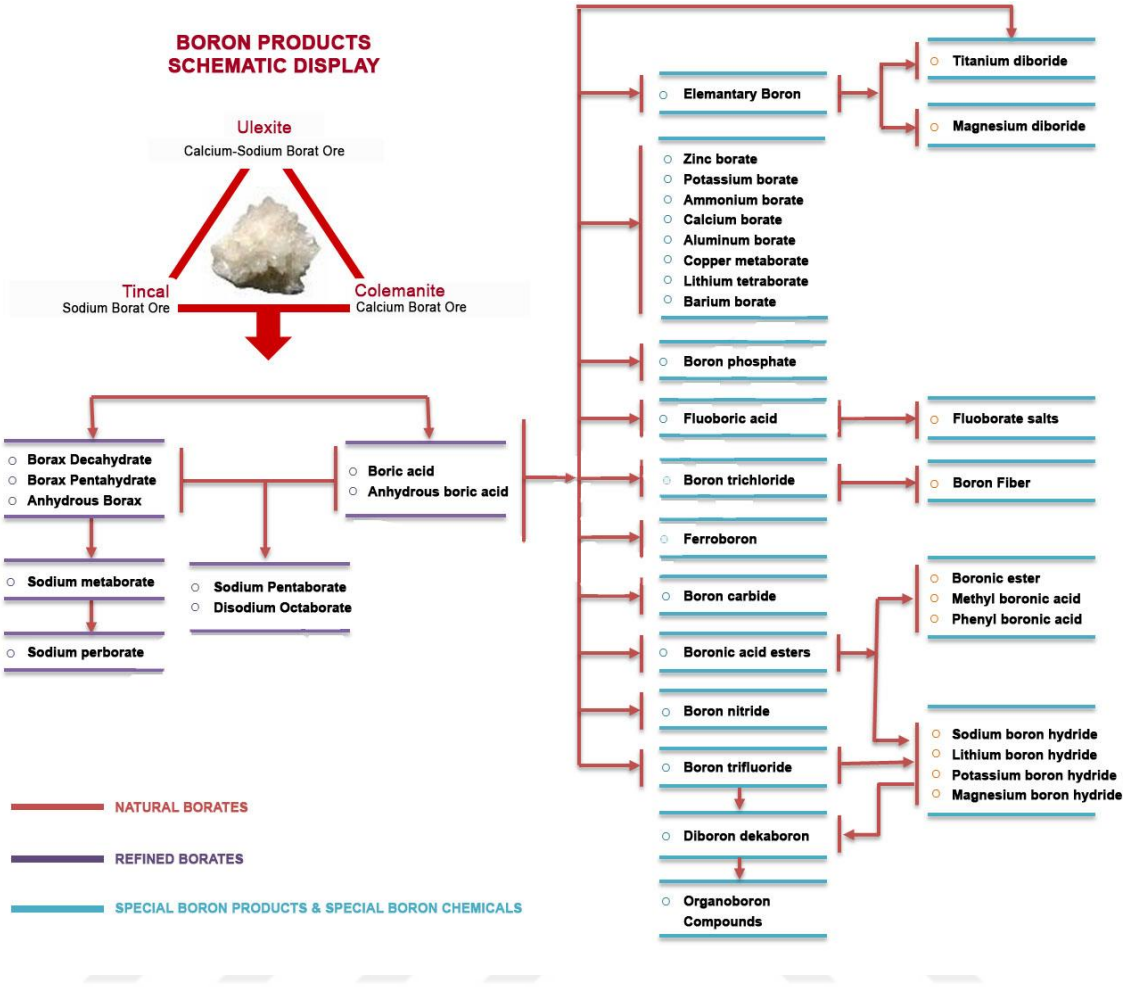


Figure 2.3 Boron Products [34]

2.3 Boron Carbide

Boron carbide is the general name for covalently bonded compounds made by boron and carbon [35]. It is also called black diamond [36]. Its general formula is B_4C. It is the hardest material known after diamond and cubic boron nitride [36], [37] . It was first discovered in 1858. In 1883, Joly was prepared cytochiometrically as B_3C. In 1894, it was named B_6C by Moissan. Boron carbide with a boron:carbon ratio of 4:1 is commercially discovered in 1934 by Ridgway [38]–[40].

2.3.1 General Properties and Use Areas

There are many studies in the literature on stoichiometry and phases of boron carbide. In studies, boron: carbon ratio was defined between 24: 2.57 and 6.5: 4. The most commonly mentioned phases are B_6C, B_3C and $B_{12}C$ [38], [41].

Boron-carbon phase diagram is given in Figure 2.4. Stoichiometrically based solid boron-carbon solution contains 9-20% carbon. The carbon content is up to 10% depending on the temperature. In systems containing less than 9% carbon, the melting point decreases with excess boron. In phases containing more than 20% carbon, the melting point decreases as graphite formation occurs. There is a decrease in mechanical properties due to graphite formation [41], [42].

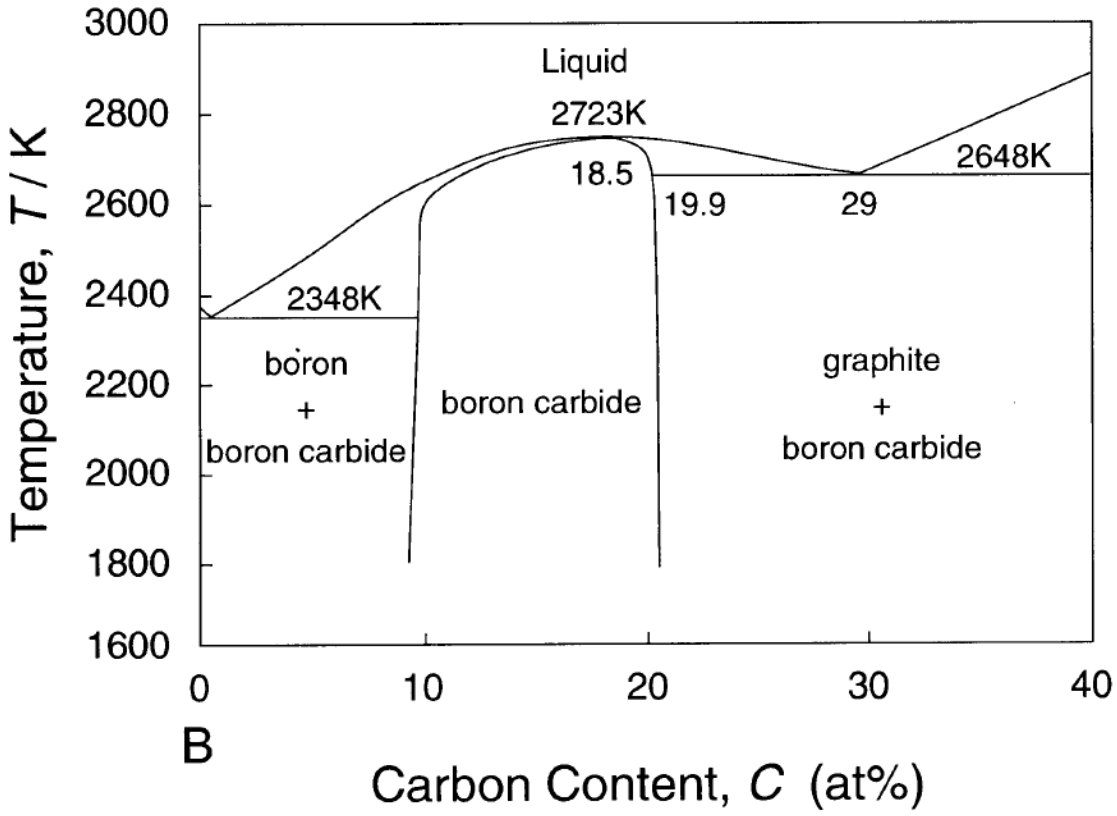


Figure 2.4 Boron – Carbon Phase Diagram [43], [44]

General features of B_4C are given in Table 2.5. The crystal structure of B4C is rhombohydral [45], [46] (Figure 2.5). Unlike B_4C, diamond and cubic boron nitride (c-BN), it can retain its hardness at high temperatures. It achieves this advantage with its rhombohedral crystal structure, which is one of the complex structures formed by boron's missing electrons. In addition, B_4C shows inertness against acids. One of the most important features of B_4C is its low density. It stands out in density-performance criteria due to its superior properties compared to advanced ceramics and metals, depending on the area of use [4], [21], [35], [47] .

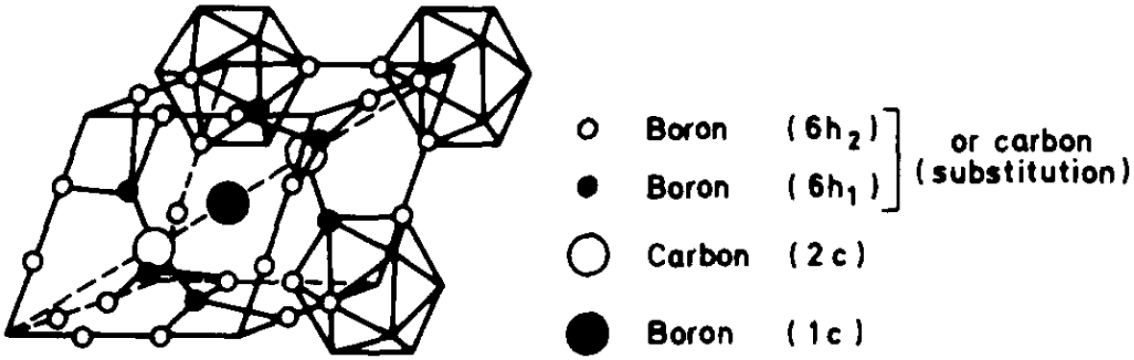


Figure 2.5 Crystal Structure of B_4C [38]

Table 2.5 General Properties of B_4C [4], [21], [35], [39], [47]

Properties	Value
Melting Point (°C)	2450
Boiling Point (°C)	>3500
Density (g/cm^3)	2.52
Hardness (HV - kg/mm^2)	3770
Fracture Toughness ($MPa.m^{1/2}$)	2.9-3.7
Poisson Ratio	0.18
Elasticity Modulus (GPa)	471
Thermal Conductivity (J/K.s.cm)	140
Thermal Expansion Coefficient	$4,5 \times 10^{-6} K^{-1}$
Neutron Absorption Cross Section (barn)	600

Besides its superior features, B_4C has some disadvantages. It has low fracture toughness and limits the usage areas of B_4C due to its low sinterability. B_4C have to be sintered at high temperature (>2000 °C) to show its superior mechanical propertie [48], [49].

B_4C is preferred in many areas of the industry due to its superior properties. The sectors where B_4C is widely used and reasons for preference are as follows [4], [21], [35], [47], [50]–[52]:

- Manufacturing Industry: Abrasive, cutting tool, jet nozzle (high hardness)
- Metallurgy: Furnace refractory, surface coating (high temperature and chemical resistance)
- Defense Industry: Ballistic protection (high hardness and low density)
- Nuclear Energy: Reactor wall brick, waste storage units (high temperature and chemical resistance, high neutron absorption ability)

2.3.2 Synthesis Methods

Synthesis studies of boron carbide started in 1883 and 1894 by Joy and Moisson respectively [21], [38]–[40]. Boron carbide synthesis methods are generally for obtaining microsized powder products. Fiber and nanoscale productions are being tried in new studies. Commercially produced boron carbide is produced by the "carbothermic reduction" method (2.1). Boric acid reacts endothermic with graphite (C) as the carbon source at 1500-2500 °C and B_4C is obtained [21], [39], [47].

$$2\ B_2O_3 + 7C \rightarrow B_4C + 6\ CO \qquad (2.1)$$

Except from the carbotermic reduction method, there are methods such as magnezothermic reduction and chemical vapor deposition (CVD). However, these production techniques are not suitable for mass production. Except from the specified production methods, there are polymeric and magnesiothermic methods that are in the development stage [21], [39], [47]. There are also studies on the synthesis of boron carbide at low temperature [3], [53].

2.4 Calcium Hexaboride

Calcium hexaboride, one of the alkali metalborides, is the most stable compound formed by calcium and boron. Other compounds are CaB_4 and CaB_2 [9], [54]. It consists of 6 B and 1 Ca atoms (Figure 2.6). In the literature, it is also called calcium boride. Calcium hexaboride is a metalic, oxygen-free, refractory metal boride

compound. Although it was first synthesized by Stackelberg in 1932, its industrial use began in the 1960s [8], [9], [54].

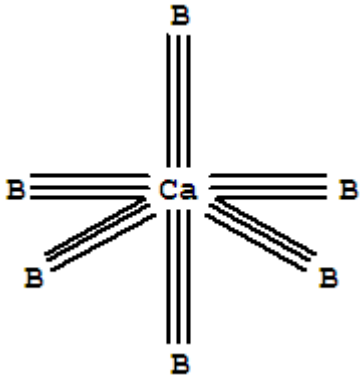


Figure 2.6 Bonding Structure of CaB_6

2.4.1 General Properties General Properties and Usage Areas

Phase diagram of B-Ca system depending on mass and atomic percent are given in Figure 2.7. The compound consists of 38% Ca by mass. In phases containing less Ca (<38 wt%), α-B and β-B phases are observed. In systems containing more than 38 wt% Ca, fcc-Ca and bcc-Ca are formed depending on the temperature [55].

CaB_6 has a cubic structure (Figure 2.8). Similar to B_4C, it contains two different lengths of Boron-Boron bonds. B-B bonds are the source of the superior mechanical and chemical properties of CaB_6 [11], [56].

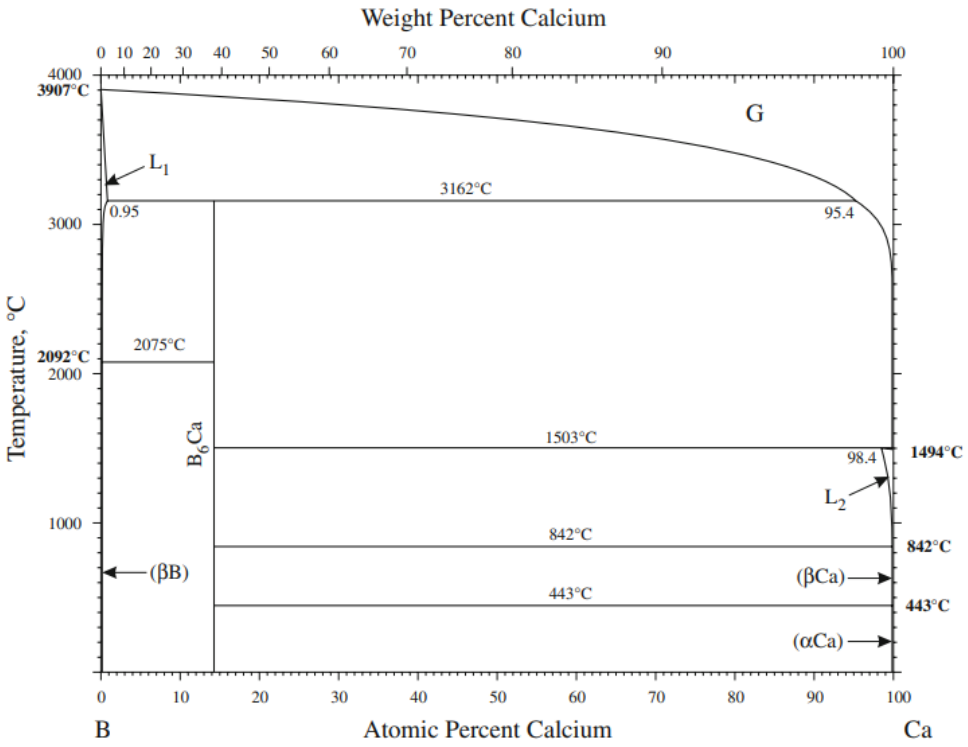


Figure 2.7 B-Ca Phase Diagram by atomic percent and weight percent of Ca [57]

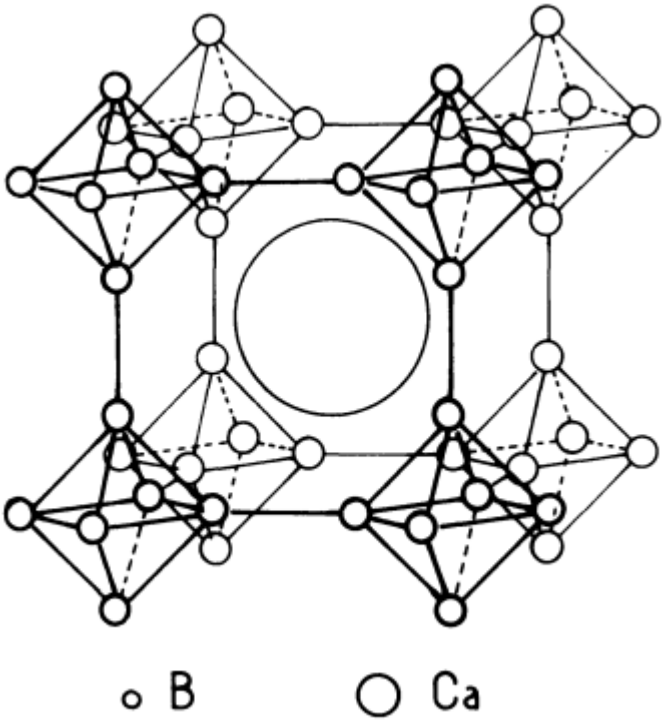


Figure 2.8 Crystal Structure of CaB_6

Most important properties of CaB_6 are its low density (2.45 g/cm^3), high hardness (27 GPa HV) and high melting point (2235 °C). Its mechanical, chemical and physical properties are summarized in Table 2.6 [13], [17], [56], [58].

Table 2.6 General Properties of CaB_6 [13], [17], [56], [58]

Properties	Value
Density (g/cm^3)	2,45
Molecular Mass (g/mol)	104,944
Melting Point (°C)	2235
Young's Modulus (GPa)	379
Harndess (HV - kg/mm^2)	25,49
Fracture Toughness (MPa.m$^{1/2}$)	3,78
Thermal Conductivity (Wm^{-1}.K^{-1})	70
Thermal Expansiyon Coefficient	6,5 x 10^{-6} K^{-1}

Due to its advanced mechanical and chemical properties, calcium hexaboride is used in many applications in the industry:

- Metallurgy: Deoxidant, boron nitride (BN) and boron trichloride (BCl_3) production raw material, refractory brick in copper refining
- Manufacturing: Abrasive, Cutting tool tip
- Nuclear Energy: Neutron absorber brick
- Electronic: n-type thermoelectric material
- Electricity: Ferromagnetic material

2.4.2 Synthesis Methods

CaB_6 can be synthesized by many methods. But these are mostly laboratory scale. Commercially produced CaB_6 is produced by the reduction of metals in the

carbothermic reactions of boron carbide. Except from this, it is produced by direct reaction of elements (2.2), reduction of metal oxides (2.3) and electrolysis method (2.4). CaB_6 formation reactions according to methods [11], [56], [59], [60]:

- Direct elemental reaction

$$Ca + nB \rightarrow CaBn \ (1700\ °C) \quad (2.2)$$

- Reduction of metal oxides with boron or boron-carbon

$$CaO + nB \rightarrow CaB_6 \quad (2.3)$$

- Carbothermic reduction

$$CaO + 3B_2O_3 + 10C \rightarrow CaB_6 + 10\ CO\ (1700\ °C) \quad (2.4)$$

- Boron carbide method

$$2CaCO_3 + 3B_4C + C \rightarrow 2\ CaB_6 + 6\ CO\ (1400\ °C) \quad (2.5)$$

3
SINTERING AND CERAMIC COMPOSITES

3.1 Sintering

The materials demonstrate their superior mechanical properties when they form a compact structure, not in powder form. Sintering is a term used in powder metallurgy and is defined as the formation of a bond between these particles by combining the powders with the help of thermal energy. In sintering, which is one of the powder metallurgy production methods, a more dense structure is obtained by courtesy of the combination of thermal energy with diffusion and particles by courtesy of the high grain boundary movement in the grain boundary in relation to the powder size [61], [62]. Sintering process is shown schematically in Figure 3.1.

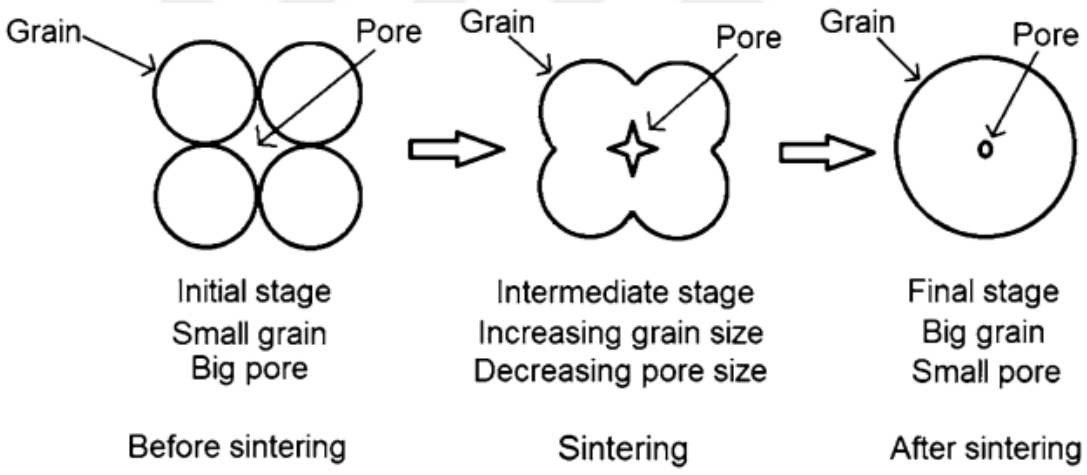


Figure 3.1 Schematic Drawing of Sintering Process [63]

Sintering is based on the phenomenon of heat and mass transport and reducing of free-energy. The factors that affect the free energy reduce that accelerates the sintering process are called the driving forces. The driving forces are particle curvature, pressure, and chemical reaction [61]. The contact points between the grains are increased by mass transport. With the help of temperature, free energy of the grains is reduced and mass transfer is accelerated. Two results are obtained by mass transfer during the sintering process: atom diffusion and/or grain coursing. Atom diffusion is defined as the atom transport to grain boundaries. In grain

coursing, grain is begin to necking and clustering. During grain growth, undesirable porosities may occur and mechanical properties may be reduce [61], [62].

There are many factors that affect the sintering rate and performance. The grain sizes and size distribution of the raw materials used, the grain shape, sintering ability and the impurities it contains affect sintering. Other factors affecting sintering are process originated. Temperature, heating and cooling rate, atmosphere, time, heating regime, pressure are the factors that affect sintering performance. In sintering using two or more raw material, homogenization is important [62].

Sintering mechanisms vary according to the type of raw material used and the method of process. Processes where the sintering temperature is below the melting point and without liquid raw materials are called solid state sintering. Processes that use liquid raw materials or whose sintering temperature is above the melting point of the raw material are called liquid phase sintering. In reaction sintering, raw materials are reacted during sintering to obtain a denser product. This process is also referred to as reactive sintering [61], [62].

3.1.1 Solid State Sintering

Solid state sintering is the most preferred method during sintering of advanced ceramics. This process is based on the atom diffusion principle. Atom diffusion is divided into three main type as volume diffusion, surface diffusion and boundary diffusion (Figure 3.2). Solid state sintering is explained by two spheres model (Figure 3.3) [61], [62], [64]. In this approach, material diffusion occurs due to chemical potential difference between grains and free energy. Low vapor pressure in the neck area allows material dispersion to be directed between the grains. The necking is spheroidizing over time and it is assumed that the two are clustered [61], [62], [64], [65].

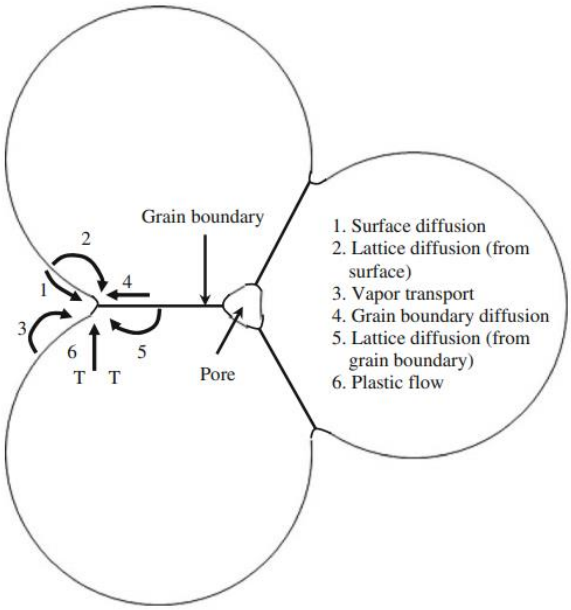


Figure 3.2 Mechanism of Diffusion and Transfer [66]

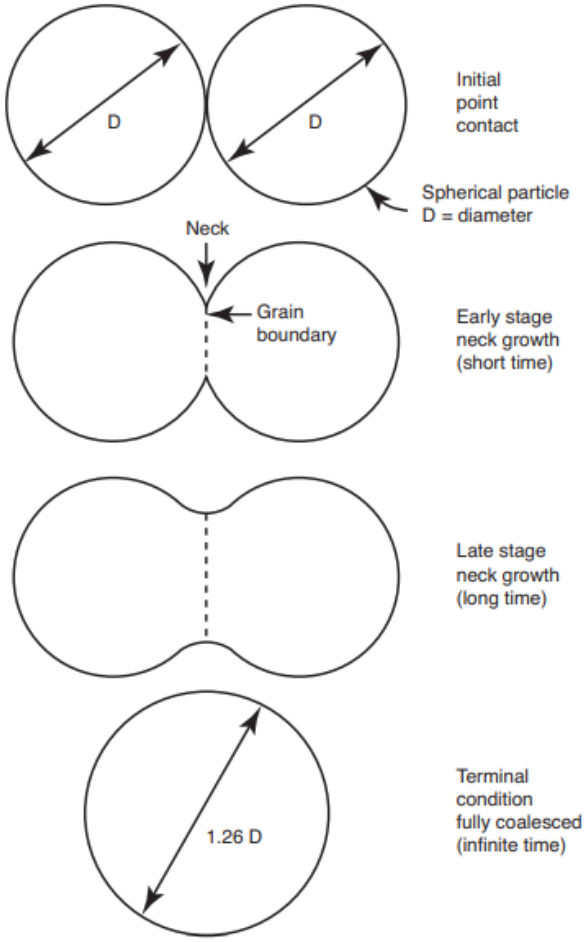


Figure 3.3 Two-Sphere Model [65]

3.1.2 Liquid Phase Sintering

Sintering temperature in liquid phase sintering is above the melting temperature of at least one of the raw materials used. The phases that melt during the sintering wet the solid powder and sintering occurs by creating a capillary effect between the powders. Liquid phases reduces porosity by reducing the surface energy of powders [61], [67].

The phase to become liquid is called the binder phase. Solid state sintering occurs until the binder phase melting. After melting, binder phase flow begins and the particles are rearranged. Solution precipitation, which accelerates condensation, occurs. Sintering continues until the condensation rate of the liquid phase equals the solid state sintering rate [61], [68].

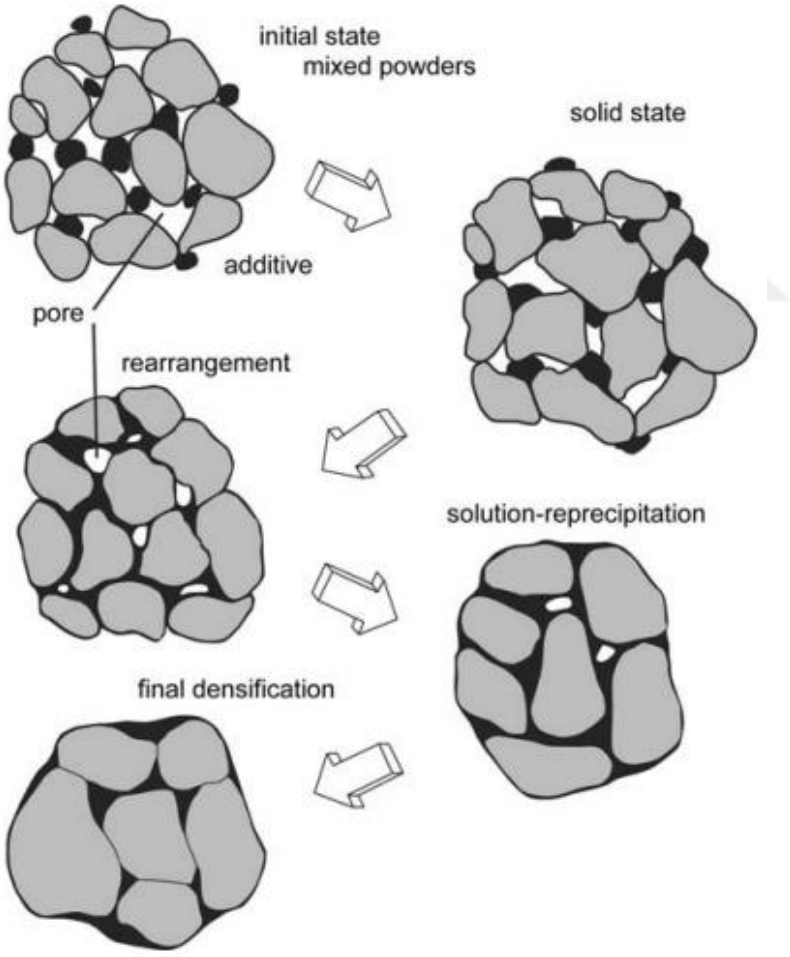


Figure 3.4 Schematically Drawing of Liquid Phase Sintering [67]

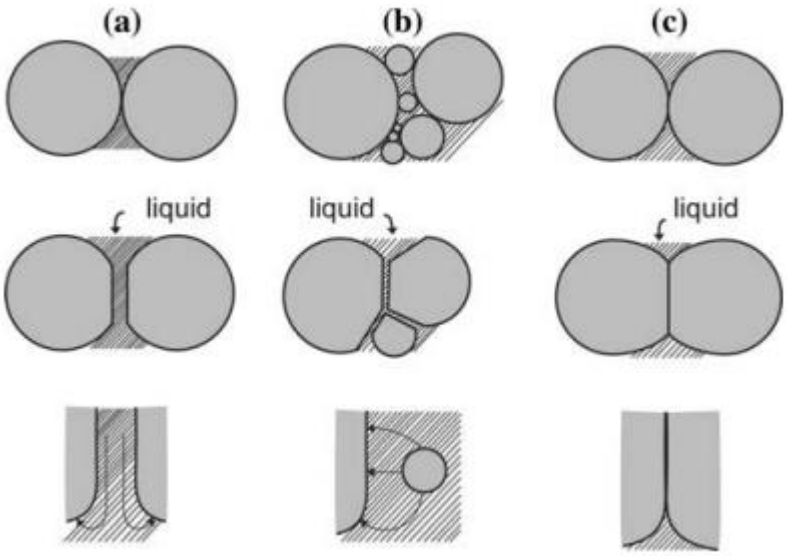


Figure 3.5 Liquid Phase Sintering Mechanism a) contact flattening b) dissolution of small grains c) solid state bonding [67]

3.1.3 Reaction Sintering

Reaction sintering is also known as reactive sintering. It takes place with at least two phases that react. Non-sintered powders react with an increase in temperature and with the pressure applied, porosity in the solid phases are aimed to be reduced. All or several phases of the sintered product can be obtained by the reaction [61].

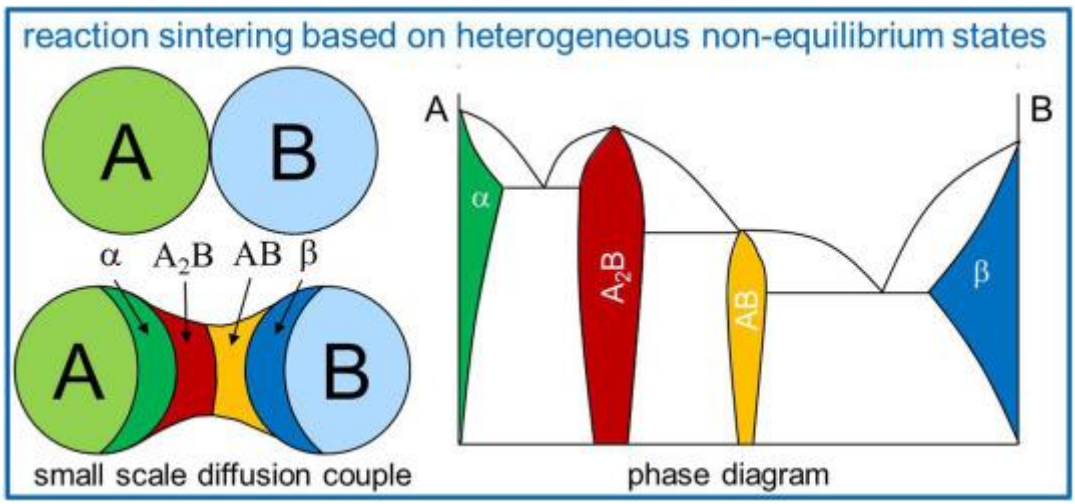


Figure 3.6 Schematecially Drawing of Reaction Sintering [69]

3.1.4 Pressure Assisted Sintering

Pressure assisted sintering is a technique developed to increase the performance or to reduce the insufficient situations of 3 basic sintering methods. In solid phase sintering, the pores can become stable and the desired density value cannot be reached. With the pressure, the porosity between the grains is reduced, the contact points are increased. The pressure assisted sintering method is a suitable method for condensing covalently bonded materials with low sinterability. Although pressure assisted sintering methods give effective results, they have disadvantages such as high production cost [62].

3.1.4.1 Hot Press

Hot press is a sintering technique performed by applying uniaxial pressure. Powders or pre-shaped parts to be sintered are placed inside the mold and placed in a press that applies pressure on one axis. During the press, the sample is heated with the help of heating elements. The applied pressure is between 10-75 MPa. The temperature may rise above 2000 °C. Graphite mold or molybdenum disilicide molds can be used as mold [61]. The hot pressing method is suitable for industrial production. Schematic representation of the hot press device is given in Figure 3.7.

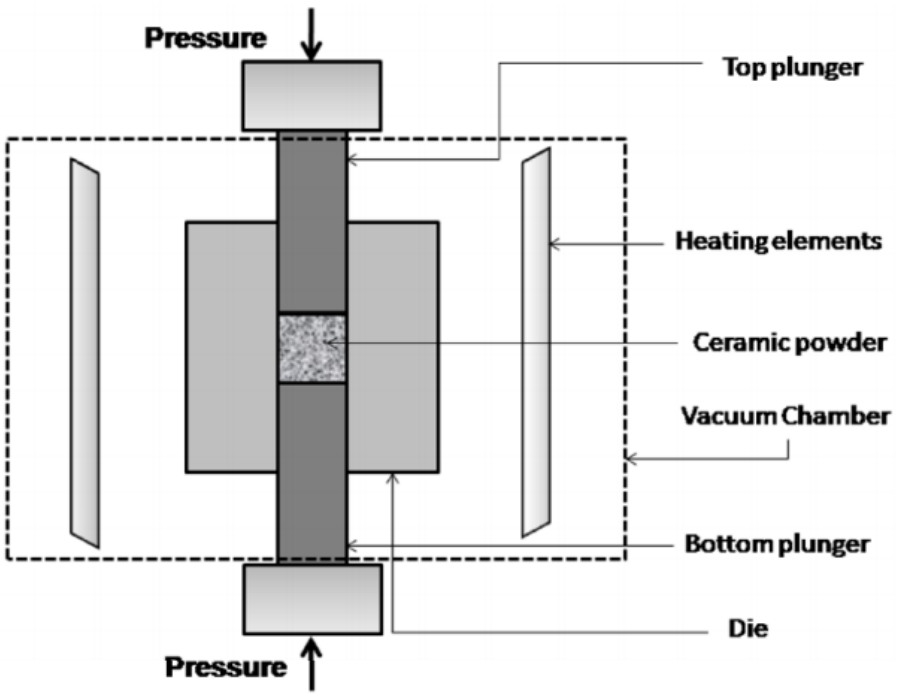


Figure 3.7 Schematic Drawing of Hot Press [70]

3.1.4.2 Hot Isostatic Press

Hot isostatic press works with a similar method to hot press. Unlike hot press, pressure is not applied from one axis and deformable mold is used. Inert gas is added to the vacuum chamber. The gas pressure is increased and brought to the desired pressure value. With the effect of gas pressure, the mold wraps around the powder and compresses the powder. With this method, shaped parts can be sintered. Unlike hot press, pressure can rise up to 200 MPa [61], [62].

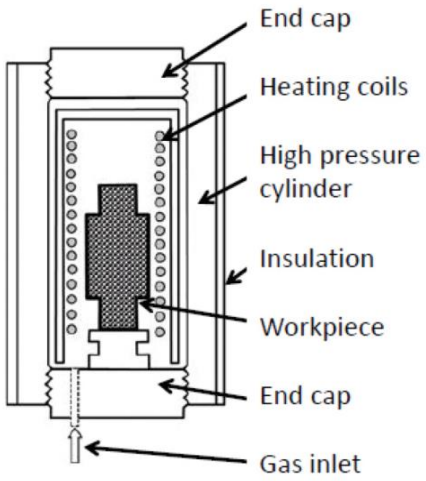


Figure 3.8 Schematic Drawing of Hot Isostatic Press [71]

3.1.4.3 Spark Plasma Sintering

Spark plasma sintering is a newer technology compared to other pressure assisted sintering methods. Powders are emitted at certain intervals and instant spark plasma formation is provided at high temperatures. In this way, sintering will occur. These methods are not suitable for industrial production compared to other methods. SPS is suitable method for experimental studies due to repeatability, low amount of raw material usage, easy control of process parameters, high heating and cooling rates and ease of operation. Sintering mechanism of SPS is similar to HP. Therefore, HP products can be produced with the data obtained from experimental studies of SPS [61], [62], [72]–[74].

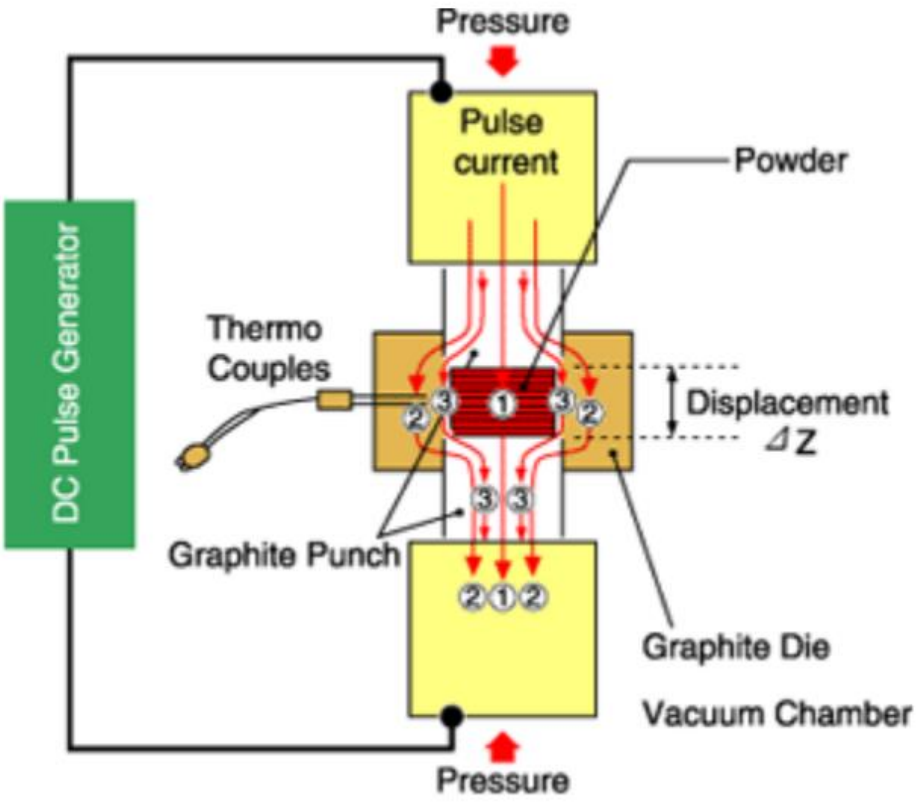


Figure 3.9 Schematic Drawing of Spark Plasma Sintering [75]

3.2 Ceramic Composites

Ceramic materials are used in many fields in the industry due to its important properties such as high temperature resistance, low density, high chemical stability, hardness, erosion and chemical resistance. Composite materials are defined as materials produced by combining two or more materials. Ceramic matrix composites are produced to eliminate the disadvantages such as low fracture toughness and low sinterability while maintaining the superior properties of ceramics [76], [77].

B_4C has low fracture toughness. Therefore, its usage area is limited. In addition, covalent bonds that provide high hardness make sintering difficult. The density of B_4C sintered without pressure does not exceed 80% of its theoretical density at 2100-2200 °C. In pressure assisted sintering methods, monolithic B_4C should be sintered at high temperatures. Also, high temperature holding time should be long for densification. (>2100 °C for 15-45 min) [36], [78]–[81]

3.2.1 Sintering Additives of Boron Carbide

The use of additives has many effects in the production of ceramic composites[82]:

- Liquid phase formation
- Formation of a second phase and preventing grain boundary movement and grain growth
- Split of grain boundaries
- Affecting the diffusion coefficient of the solid solution of the material.
- Reduce grain boundary energy and free surface energy ratio

The most preferred method used to increase the sintering ability of B_4C and to improve its low mechanical properties is the use of sintering additive. There are many studies in the literature on B_4C sinter additives. Additives are generally divided into 3 basic groups: metallics, oxidics and non-oxide. The most commonly used sinter agents are carbon (C), boron (B), TiB_2, silicon (Si), aluminium (Al), TiC, SiC, aluminium oxide (Al_2O_3), titanium oxide (TiO_2), zirconium oxide (ZrO_2) [80], [82]–[89].

Al, magnesium (Mg), iron (Fe), B, wolfram (W), titanium (Ti) are generally used as metallic additives in the sintering of B_4C. Along with additives, 300-450 °C decrease is provided in sintering temperature.. Metallic additives react with B_4C to form new phases. The formation of new phases varies depending on the process method, temperature and duration [82], [90], [91].

During pressureless sintering at 920 °C with different amounts of Mg reaction between Mg and B_4C occurred and it was observed that MgB_2 and MgB_2C_2 phases were formed. Density decreased with the addition of Mg, but mechanical properties decreased [92], [93]ca. In the sintering studies carried out with the addition of Al, the formation of Al_3BC, AlB_2, $Al_8B_4C_7$ phases occurred. Porosity is reduced by the addition of Al. Mechanical properties are improved or reduced depending on the rate of addition [80], [89], [93]. In studies conducted with Si additive for HP at 1950°C, SiC phase formation is observed. A theoretical density of 99.2% was reached with 12% Si addition [94]. In the study that Al and Si used together,

formation of SiC, Al_4C_3 and Al_4SiC_4 phases were observed. In the study conducted without pressure sintering method, a theoretical density of 97.4% was reached at 2226 ° C [95].

Al_2O_3, yttrium oxide (Y_2O_3), TiO_2 are preferred as oxide-based sinter additives. Oxides react with the B_4C phase during sintering to form new phases and promote densification. They also reduce production costs. No reaction occurs between Al2O3 and B_4C, it takes place through the Al_2O_3-B_2O_3 phase system. Al_2O_3 additive reacting with B_2O_3 formed on B_4C grains during sintering increases density and generally improves mechanical properties by forming $AlB_{12}C_2$[B_{12}(CAlC)], $Al_{20}B_2O_{36}$, $Al_{18}B_4O_{33}$ phases at grain boundaries[96], [97]. Y_2O_3 with Al_2O_3, transform to liquid phase at low sintering temperatures (~1900 °C) of B_4C. Liquid phases $Y_3Al_3O_5$, $YAlO_3$ and $Y_4Al_2O_9$ located between B_4C grains, generate a driving force and increasing densification[98]. TiO_2 is an oxide that reacts with B_4C. The reaction started at 900 °C is completed at 1500 °C and TiB_2 is formed [99], [100]. The composite, which was sintered at 2050 °C for 30 minutes by adding 10% TiO_2, reached a relative density of 91%. Producing of B_4C-TiB_2 composite as a result of reactive sintering by adding TiO_2 instead of TiB_2 additon the structure provide to obtain a more dense structure and reduce production cost [101].

Except from metallic and oxidic additives, there are elemental additives, boride-based additives, nitride-based additives and carbide-based additives. Carbon (C) is the most commonly used elemental sintering additive. C can also be added to the composites in graphite form. C is optimum additive type in pressureless sintering. There is free C in low purity B_4C raw materials. C, which is accepted as impurity in raw material, reacts with other raw materials during sintering and improved reactive sintering [76], [82], [85], [102], [103]. B_4C-C composites, which were prepared with the addition of 4wt% C, were sintered at 2250 °C without pressure sintering. Relative density increased by 2.2 points compared to monolithic B_4C and reached 97.7%. However, mechanical properties decreased [102].

SiC and TiC are preferred carbide types additives in B_4C sintering. TiC reacts with B_4C to form the TiB_2 phase. However, in sinterings where the reaction is not homogeneous, free carbon turns into graphite and reduces mechanical properties.

[50], [104]. SiC is the most efficient compound that improves the sintering behavior and mechanical properties of B_4C among carbide-based additives. SiC does not react with B_4C during sintering and remains the secondary phase. It prevents the growth of B_4C grains that start growing with temperature. It helps uniform distribution of grain distribution. It also located at B_4C grain boundaries, affecting fracture progression and improving mechanical properties. B_4C-SiC composites are suitable for many sintering methods. However, liquid phase sintering can take place in methods that occur in in situ SiC formation. Also, the high density of SiC (3,21 g/cm^3) negatively affects the low density advantage of B_4C [105]–[107]. Except from SiC, W and tungsten carbide (WC) is used as a sinter agent. However, its use is not preferred due to its very high density (15,6 g/cm^3).

The most important of boride-based sintering additives is TiB_2. The addition of TiB_2 significantly increases the fracture toughness of the B_4C. It also increases its hardness. It has a similar mechanism with SiC. It improves mechanical properties by controlling grain growth. However, its high density (4,52 g / cm3) increases the density of the B_4C-TiB_2 composite [102], [108]–[111].

Nitride based sinter additives are silicon nitride (Si_3N_4), BN and aluminium nitride (AlN). However, these additives are not preferred [112]–[117].

3.2.2 B_4C-CaB_6

There are a limited number of studies in the literature on B_4C-CaB_6 composites. Unlike other sintering additives, the physical and chemical properties of CaB_6 are similar to B_4C. Because of the similar mechanical and physical properties of each other, sintering is easier while the loss of mechanical properties is minimized. In addition, using $CaCO_3$ as a source of CaB_6 during reactive sintering at high temperatures reduces composite production costs [16].

B_4C-CaB_6 composites containing different rates of CaB_6 in the range of 0-40 wt% were produced with a hot press at 2150 °C with 30 MPa. There were no significant changes in the densities of the composites due to their similar density of raw materials. The strength of the additive-free B_4C sample increased from 420 MPa to

425 MPa with the addition of 20wt% CaB_6. The density decreased from 2.54 to 2.52. Hardness has improved from 34 GPa HV to 38 GPa HV [16].

In another study, samples with CaB_6 added to the B_4C-Al_2O_3 composites were sintered with hot press at 1900 °C with 30 MPa. The hardness of the B_4C-Al_2O_3 (75wt -10wt%) composite containing 15wt% CaB_6 increased from 36.4 GPa HV to 39.3 GPa HV. Also, relative density increased from 92.8% to 95.9. Although CaB_6 is lower than B_4C as hardness, it caused an increase in hardness because it reduces porosity and positively affects sintering [17].

4
EXPERIMENTAL SECTION

4.1 Materials

The raw materials obtained from commercial manufacturers were used in the study. B_4C powder was supplied from Nanografi Nanotechnology (>99.5 %, 1-3μm), and CaB_6 powders from Dandong Chemical Industry Institute Co., Ltd (>99 %, 5-10μm).

4.2 Preparation of Samples

While preparing the sample mixes, the mixing ratio method was used. The powder mixtures studied are summarized in Table 4.1.

Table 4.1 Sample Designation and Compositions

Sample ID	B_4C (wt%)	CaB_6 (wt%)
B100	100	0
BC5	95	5
BC10	90	10
BC15	85	15
BC20	80	20
C100	0	100

The samples were mixed in an IPA (Shell Global, 2-propanol, purity> 99.8%) dispersant in the planetary mono mill (Fritsch Pulverisette 6) consisting of Si_3N_4 balls and jar, whose properties are given in Table 4.2 for homogenization.

Table 4.2 Homogenisation Parameters

Parameters	**Value**
Jar Type	Si_3N_4

Table 4.2 Homogenisation Parameters (Continued)

Ball Type	Si_3N_4
Ball Dimensions	Ø 10 mm
Powder:Ball Ratio	50:75
Time	60 min
Cycle	300 RPM
Dispersant	IPA (99,95% purity)

After the homogenization process, the mixtures were dried at 60 RPM in a rotary evaporator (Heidolph-HeiVAP) with a water temperature of 55 °C to evaporated of IPA. The dried mixes were sieved through a 300 μm screen.

4.3 Spark Plasma Sintering of Samples

Spark plasma sintering furnace (FCT-HP D 25/1) was used to sinter raw materials and dried mixtures. The sintering behaviors of the raw materials used in the first stage of the study were examined. Sintering at different temperatures (1900 °C and 2050 °C) was performed to examine the sintering behavior of B_4C. The sintering behavior of CaB_6 was examined at 1850 °C. The powders were weighed 5 g in accordance with the sample thickness desired to be obtained and put into a 20 mm diameter graphite mold (Morgan Advanced Materials). To prevent the sample from sticking to the mold, graphite paper was used between the punches and the sample. Molds are wrapped with graphite blankets to prevent heat loss. The prepared mold was compressed by applying 10 MPa pressure with the hand press. Compressed molds are placed on the SPS furnace. The prepared mold-sample system is schematically shown in Figure 4.1.

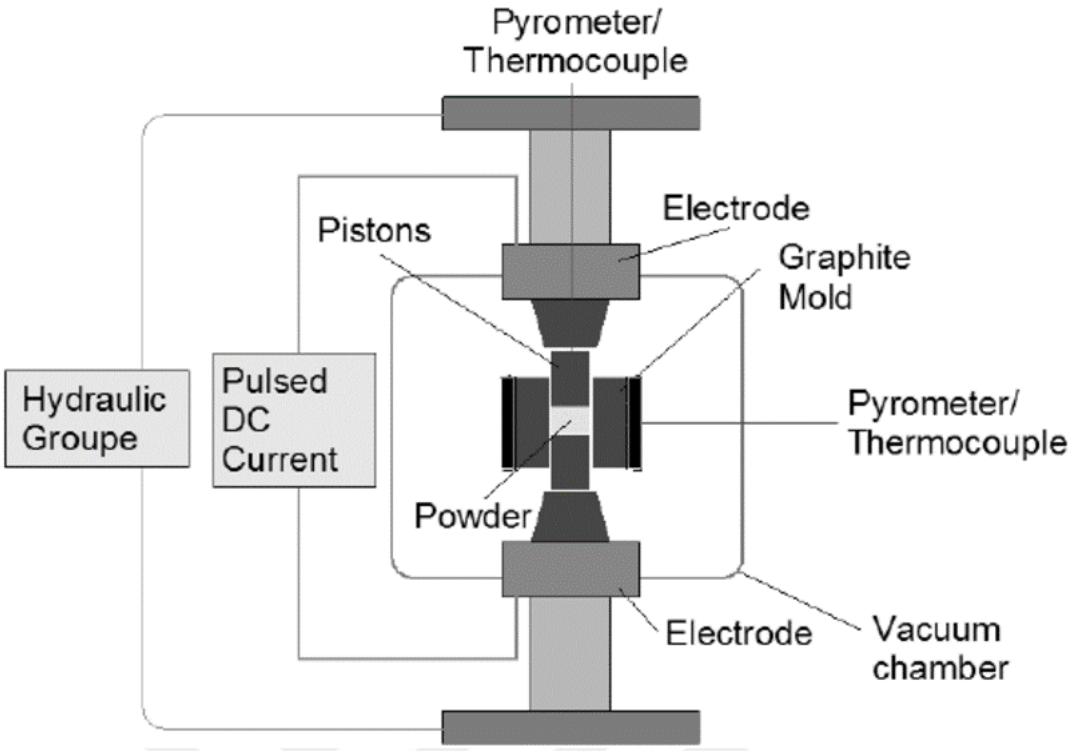


Figure 4.1 Schematic Representation of the Mold System Used in SPS [118]

During sintering, all parameters were monitored on the computer screen. Samples placed in the device were heated at 100 °C/min. 10 min was waited at the maximum temperature. Furnace cooling was carried out by power shutdown. During the entire sintering period, 30 MPa pressure was applied to the graphite molds. Samples were sintered with the parameters given in Table 4.3.

Table 4.3 Sintering Parameters

Parameters	Value
Pressure (MPa)	30
Heating Rate (°C/min)	100
Maximum Temperature (°C)	1900 – Mixed Powder 1900-2050- Monolithic B_4C 1850- Monolithic Ca_B6

Table 4.3 Sintering Parameters (Continued)

Holding Time (min)	5
Pulse Time (ms : ms)	12:2
Atmosphere	Vacuum (1 kPa)

The sintering temperature of the mixtures was determined as 1900 °C as a result of the analysis of the sintering behavior of monolithic B_4C. The mixtures were sintered with the parameters given in Table 4.3 in a experimental flow similar to monolithic sintering.

5
CHARACTERIZATION STUDIES

5.1 Characterization of Raw Materials

XRD (Rigaku Miniflex 600, CuKα, 40 kV, 15 mA, 10° – 70°) and SEM-EDS (SEM- FEI Quanta FEG 450 equipped with EDAX EDS) analysis were performed to characterized of the raw materials.

5.2 Sintering Ability

SPS furnace records the vacuum value, temperature, pressure, current, voltage values of the device during sintering, shrinkage rate of the sintered sample, the amount of shrinkage parameters. Shrinkage is defined as the distance between graphite-based punches that compress the sample powders. Depending on the addition of sintering agent, shrinkage rate and sintering start-end temperatures change. Sintering behaviors of the samples were analyzed with the CaB6 Ratio-shrinkage-temperature parameters.

5.3 Density and Open Porosity

Archimedes method is used for density and open porosity measure. Sintered samples were suspended in boiling distilled water for 3 hours and the air remaining in the pores was removed. The suspended weight is W1 and the wet weight is W2. Samples were dried in an oven of 100 °C for 1 h to remove the distilled water accumulated in the pores. The dry weight was recorded as W3. Experimental density was calculated using equation 5.1, and open porosity using equation 5.2.

$$Experimental\ Density\ (g/cm^3) = \frac{W_3}{W_2 - W_1} \times \rho_{water} \qquad (5.1)$$

$$Open\ Porosity\ (\%) = \frac{W_2 - W_3}{W_2 - W_1} \times 100 \qquad (5.2)$$

Mixture rule was used to calculate theoretical density of B_4C-CaB_6 mixtures (Equation 5.3).

$$\rho_{theoratical} = (V_{matrix} \times \rho_{matrix}) + (V_{additive} \times \rho_{additive}) \qquad (5.3)$$

5.4 XRD Phase Analysis

Sintered samples were milled by ring mill (Rocklabs Rocklabs BenchTop Ring Mill Pulveriser) equipped with WC-Co ring and chamber for XRD analysis. To identify crystal structure of samples, XRD (Rigaku Miniflex 600) analysis was performed. Analyses were carried out with 40 kV acceleration voltage and 15 mA current by CuKα radiation. Samples were characterized between 10° – 70°.

5.5 Microstructural Analysis

Samples were cut with a precision cutting device (Struers-Secotom 1) for microstructure analysis. The cut samples were taken into hot bakelite mold (Struers-LaboPress, 150 °C). The molded samples were polished for analysis with an automatic polishing device (Struers-TegraPol 25). Polishing steps are rough, 9, 6, 3 and 1 μm diamond solution and diamond. Microstructures of sintered samples were characterize by scanning electron microscopy (SEM) FEI Quanta FEG 450 equipped with EDS-EDAX. Samples were first coated with a mix of Pd and Au by Quarum SC7620 Mini Sputter Coater/Glow Discharge System to prevent electron charging on sample surface.

5.6 Mechanical Tests

Hardness and fracture toughness of sintered samples were measured. Polished sample surfaces were used for SEM-EDS analysis. Vickers micro hardness device (Emcotest-M1C 010) was used for hardness measurement. The diamond indenter with a pyramid angle of 136° was applied to the sample surface for 10 seconds with a load of 5 kg. Hardness measurements were made 3 times for each sample and the average value was taken. The method used to calculate the hardness is given in equation 5.4. The result of the calculation is in the GPa unit. F in the formula represents the applied force (N) and a represents the diagonal length (μm) of the resulting test result.

$$HV = \frac{0{,}47 \times F}{a^2} \tag{5.4}$$

Crack lengths obtained as a result of the Vickers test were measured under an optical microscope. The fracture toughness was calculated using the equation developed by Niihara (Equation 5.5). In the formula, K_{IC} refers to fracture toughness

(MPa.m$^{1/2}$), E is Young's Modulus (MPa), HV is vickers hardness (GPa), a is diagonal length (μm), c crack lengths (μm).

$$K_{IC} = 0{,}067 \times \left(\frac{E}{HV}\right)^{0{,}04} \times HV \times a^{0{,}5} \times \left(\frac{c}{a}\right)^{-1{,}5} \quad (5.5)$$

6
RESULTS AND DISCUSSIONS

6.1 Characterization Results of Raw Materials

Figure 6.1 shows XRD patterns of raw materials. Characteristic B_4C peaks can be seen in the boron carbide powders patterns. Titanium carbide (TiC) ve titanium oxide (TiO_2) peaks are present as inclusion (Figure 6.1). TiC may be contaminated from balls during grinding after synthesis of B_4C. TiO_2 is caused by oxidized TiC. The particle size distribution is seen in SEM images (Figure 6.2-a). The average particle size is in the range of 1-3 microns. Oxygen is seen on the powder surfaces as a result of oxidation (Figure 6.2-b).

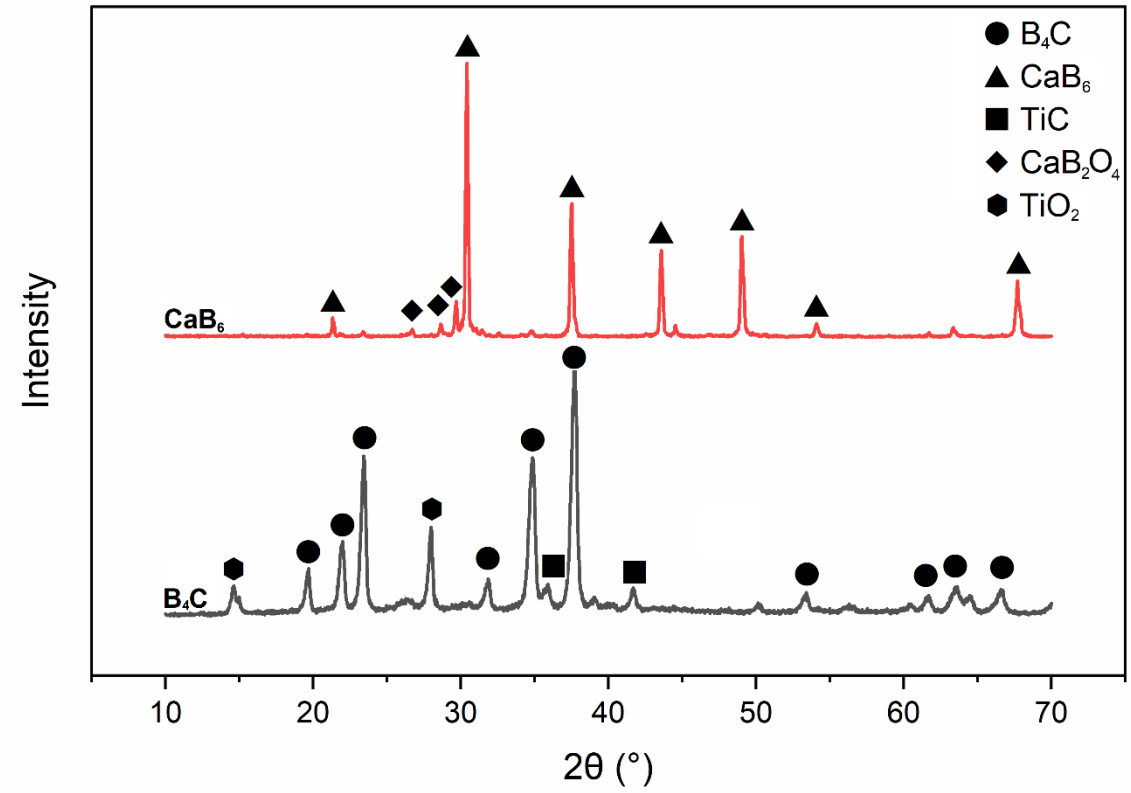


Figure 6.1 XRD Patterns of Raw Materials

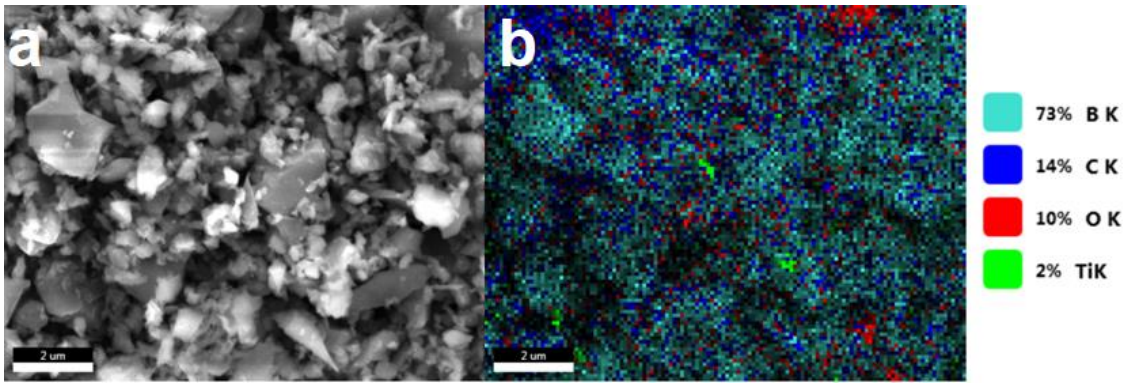


Figure 6.3 SEM Image of Boron Carbide Powder and EDS Mapping Results a) Secondary Image b) EDS Mapping Illustration

Table 6.2 EDS Analysis of Boron Carbide Powders

Elemental	Weight %
B K	76.40
C K	21.70
O K	1.73
Ti K	0.17

Figure 6.1 shows CaB_6 powders XRD pattern. Except for characteristic CaB_6 peaks, calcium borate (CaB_2O_4) peaks are detected. CaB_2O_4 may originate from oxidized CaB_6 powders during synthesis or storage. Figure 6.3 shows back scattered electron image of calcium hexaboride powders. Average grain size varies between 5-10 microns (Figure 6.3). In addition, iron is present as impurity (Table 6.2). Oxygen signals from the oxidation of the powder were detected.

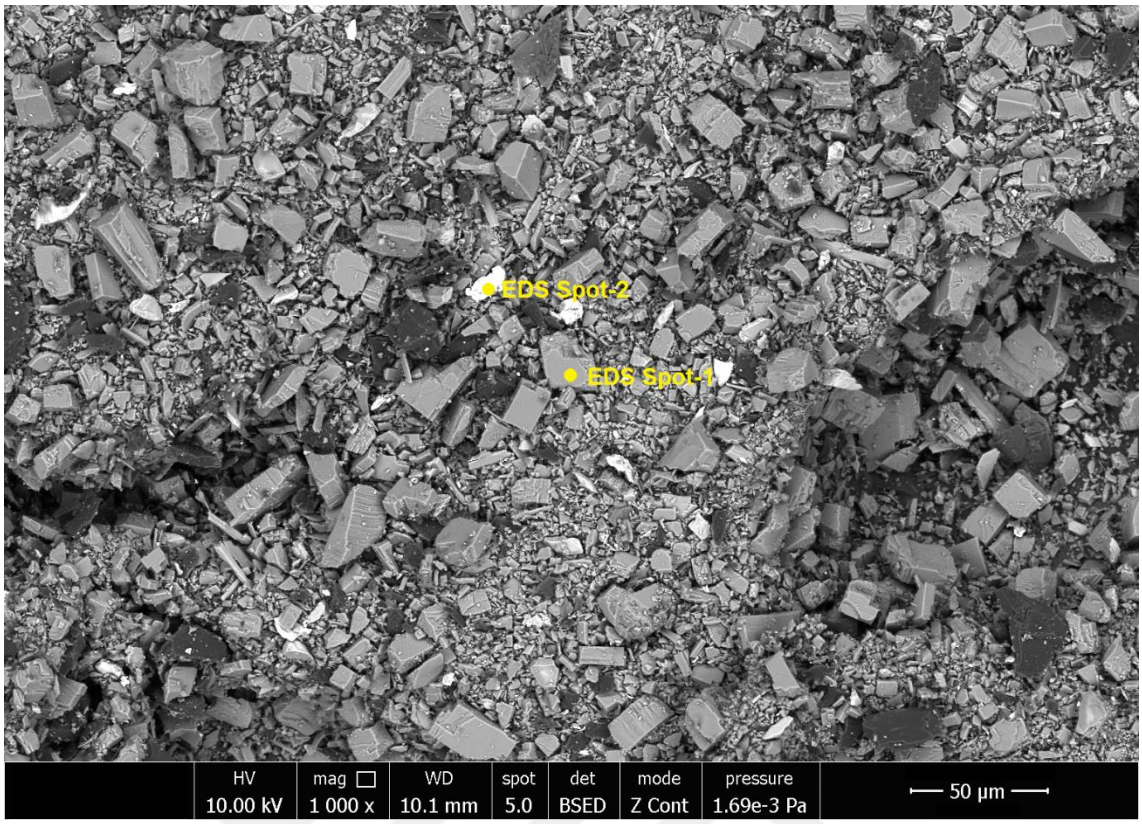


Figure 6.3 SEM Image of Calcium Hexaboride Powders

Table 6.2 EDS Analysis of Calcium Hexaboride Powders

EDS Spot-1		EDS Spot-2	
Elemental	Weight %	Elemental	Weight %
B K	61,37	B K	24,16
O K	0,08	O K	5,96
Ca K	38,56	Fe K	67,12
		Ca K	2,75

6.2 Sintering Behaviour of B_4C at Different Temperature

Boron carbide powders without additives were sintered for 10 minutes at 1900 °C and 15 minutes at 2050 °C to analyze the sintering behavior of B_4C at different temperatures. Figure 6.4 shows the time-temperature-shrinkage plot of the B_4C sample sintered at 2050 °C. During the first 200 s, the air gaps in boron carbide powders were reduced by the press. Therefore, shrinkage is observed. Air gap shrinkage was completed at 900 °C under the influence of pressure. Sintering did not occur until the temperature reached 1430 °C. While sintering was slow until

1700 °C, then the shrinkage rate increased due to temperature increase. After the temperature reached 1900 °C, the shrinkage rate and amount decreased. It reached its maximum sintering at 2050 °C within 2 min. Due to the remarkable change at 1900 °C, it was decided to sintering of CaB_6-added samples at 1900 °C for 10 minutes.

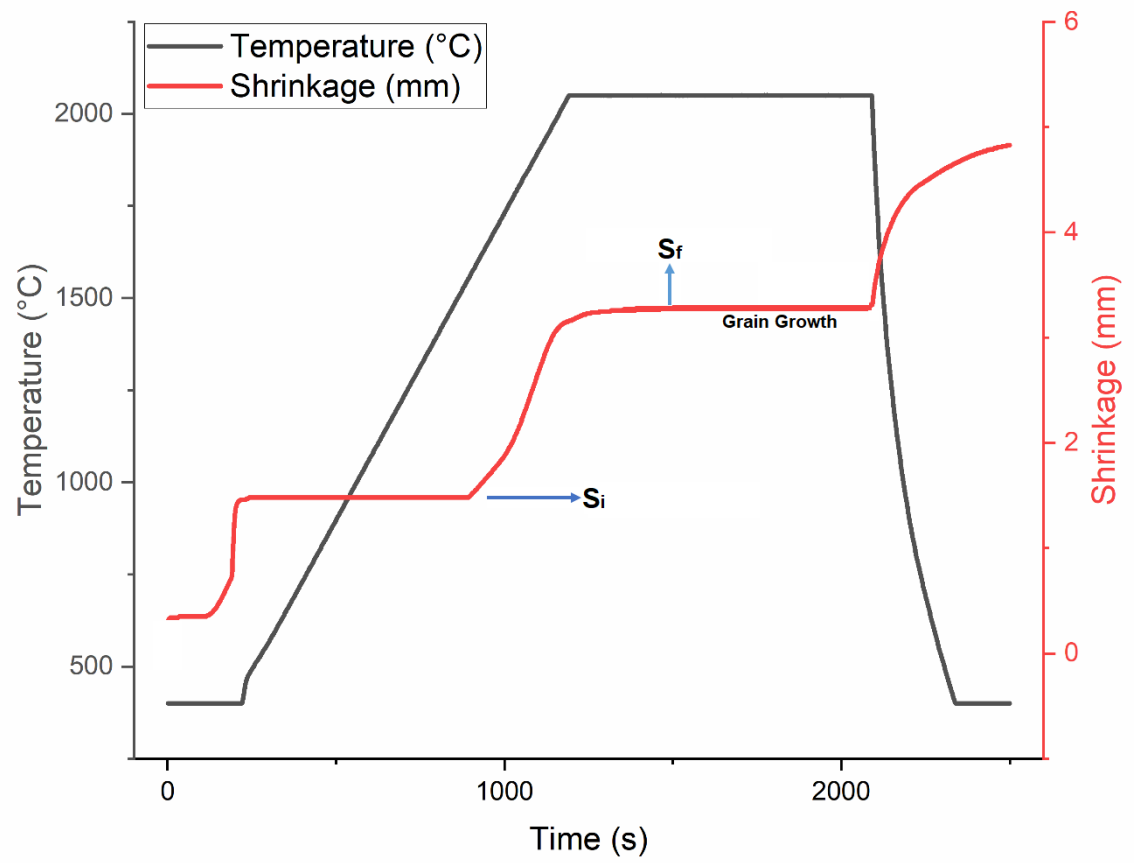


Figure 6.4 Sintering Curve of B100 Sample at 2050 °C

Figure 6.5 shows the sintering behavior of monolithic B_4C powder sintered at 1900°C for 10 minutes. It has a sintering graph similar to the B_4C sample sintered at 2050°C. It reached its maximum sintering at 1900°C within 4 minutes. The remaining 1 minute from the holding time is the stage of grain growth.

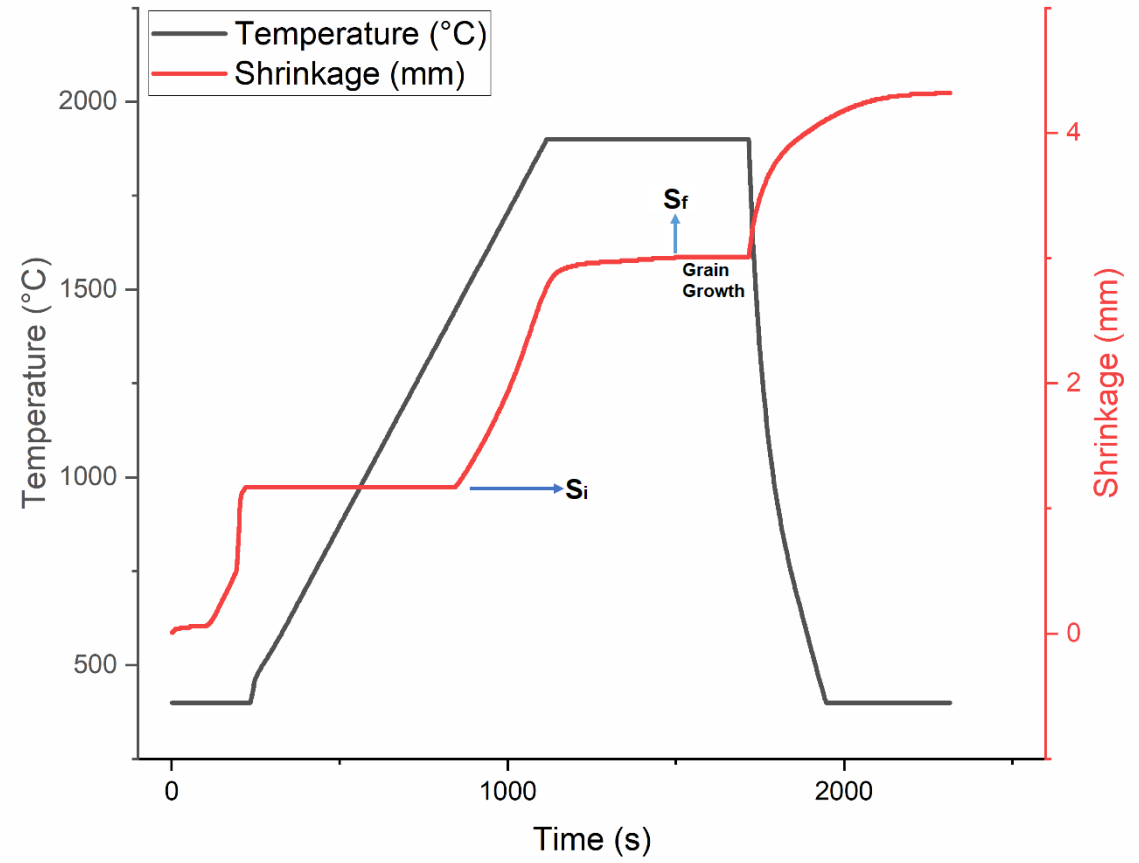


Figure 6.5 Sintering Curve of B100 Sample at 1900 °C

6.3 Sintering Behaviour of CaB_6

The sintering behavior of CaB_6 is given in Figure 6.6. Shrinkage is observed due to the decrease in the gap between powders due to the pressure of 30 MPa for the first 200 seconds. CaB_6 started sintering at 900 °C and was sintered at low speed until the temperature reached 1500 °C. After the temperature exceeded 1500 °C, the sintering rate increased. Maximum sintering at 1850 °C was reached in 8 min. Sintering of CaB_6 was easier than B_4C, because of CaB_6's Ca-B bonds are weaker than B_4C's B-C bonds.

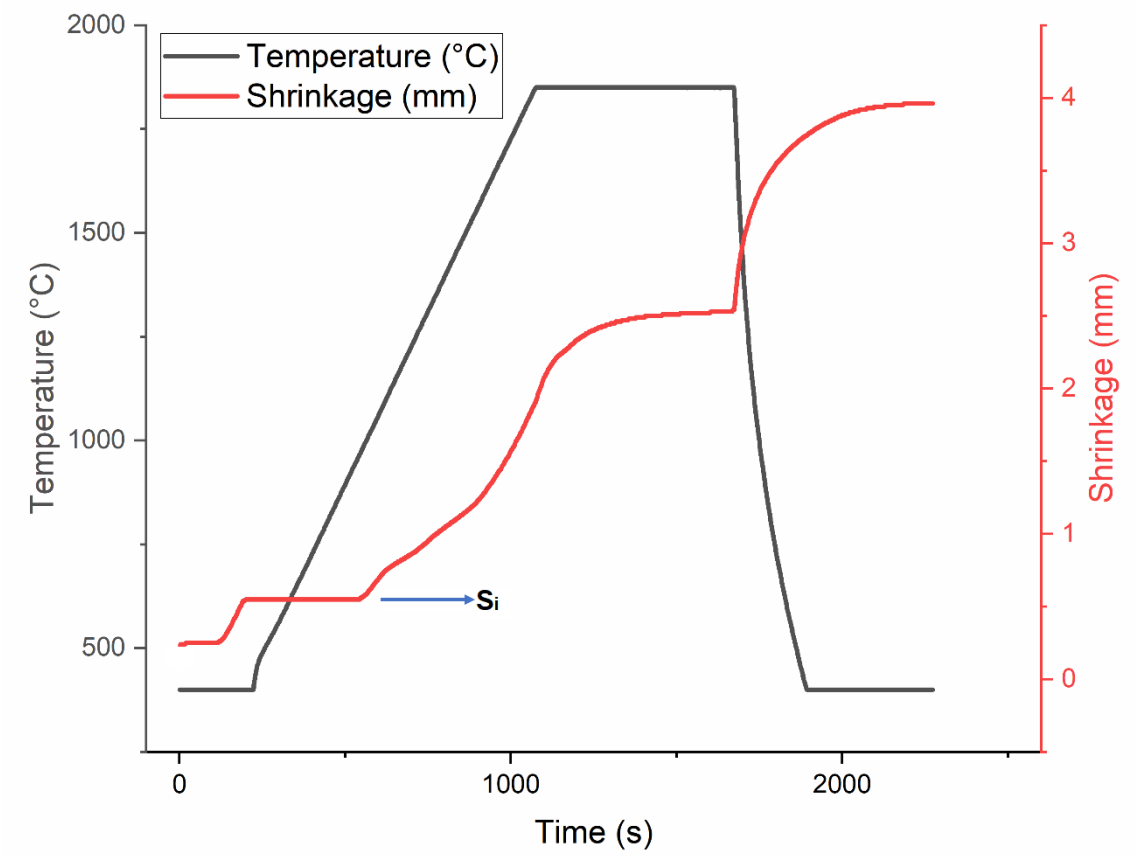


Figure 6.6 Sintering Curve of C100 at 1850 °C

6.4 Effect of CaB_6 Ratio on Sintering Behaviour of B_4C

SPS furnace shrinkage graph was used to investigate the effect of CaB_6 ratio on composite sintering behavior of B_4C-CaB_6 composites. Similar to the previous sintering, mechanical effected shrinkage is observed in all samples with the effect of the press for the first 200 s. The shrinkage graph of the sample containing 5wt% CaB_6 is shown in Figure 6.7. The sintering initial temperature decreases by 10 °C compared to the B100 sample without additives. It took 150 s longer for the BC5 sample to reach its maximum density at 1900 °C compared to the B100 sample.

The 10wt% CaB_6 additive caused a 30 °C lower in sintering temperature. However, reaching the maximum density at 1900 °C was 60 s earlier than the BC5 sample. The sintering of CaB_6 was easier compared to B_4C, which positively affected the sintering behavior of the composite. There were remarkable changes in sintering behavior with the contribution rate exceeding 10wt% (Figure 6.8). Increasing CaB_6 ratio in B_4C matrix caused a significant decrease in sintering temperature.

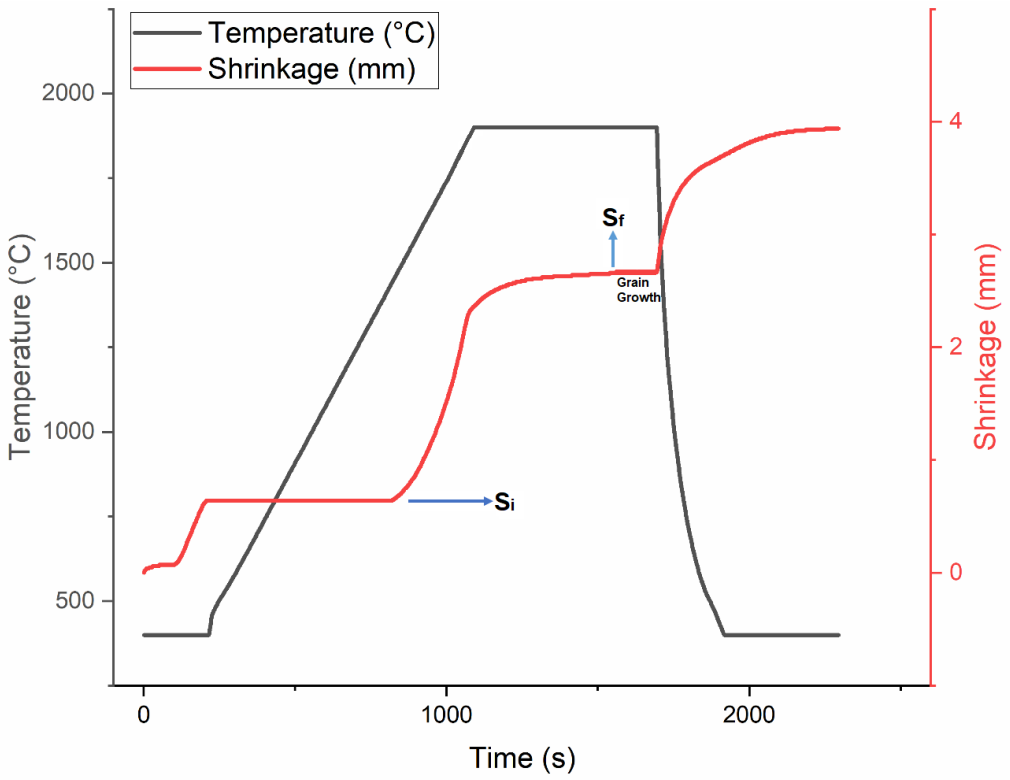


Figure 6.7 Sintering Curve of BC5 Sample at 1900 °C

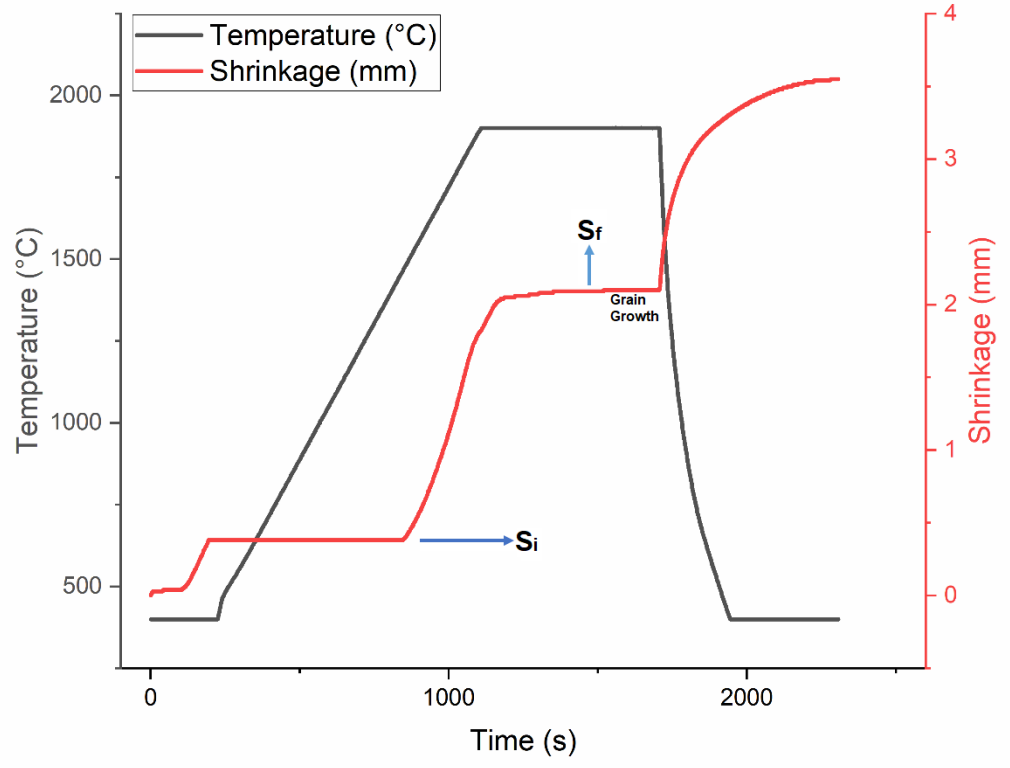


Figure 6.8 Sintering Curve of BC10 Sample at 1900 °C

Figure 6.9 shows the sintering behavior of the BC15 sample. Sintering started at 1300 °C. Sintering rate remained constant until the temperature reached 1900 ° C. Figure 6.10 shows the sintering behavior of the BC20 sample. Increased ratio of CaB_6 in the B_4C matrix caused a decrease in initial sintering temperature to 330 °C. After reaching 1430 °C, which is the initial sintering temperature of the monolithic B_4C, there was a small increase in sintering rate. The BC20 sample has reached its maximum density at 1900 °C earlier than the BC15 sample.

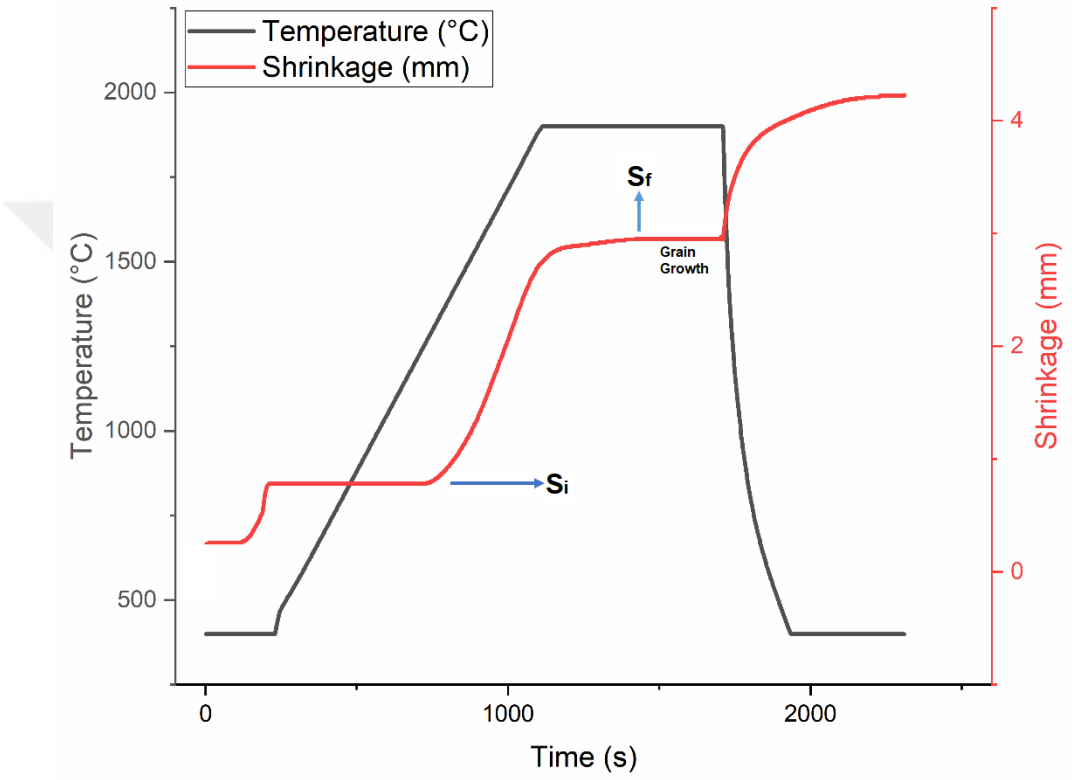


Figure 6.9 Sintering Curve of BC15 Sample at 1900 °C

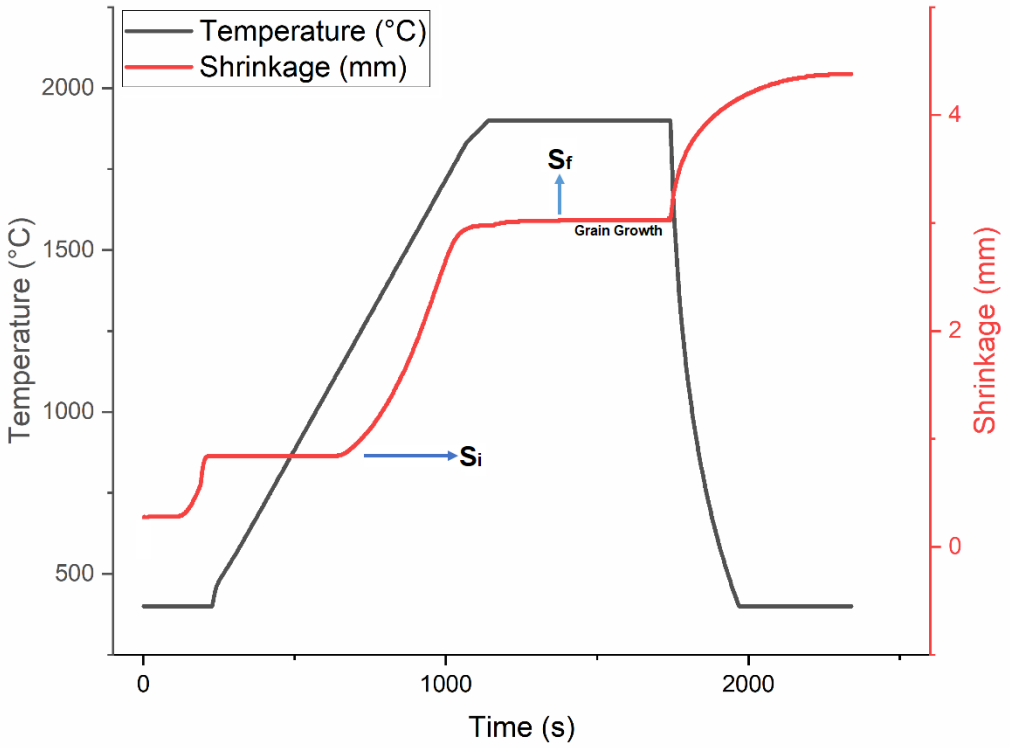


Figure 6.10 Sintering Curve of BC20 Sample at 1900 °C

6.5 Density and Open Porosity

Densities and open porosities of the samples after sintering were measured with the archimedes principle. The results are given in Table 6.3. The B_4C sample sintered at 2050 °C approached its theoretical density. However, by lowering the sintering temperature by 150 °C, B_4C could not reach its theoretical density. The increase in apparent porosity indicates that the sample was not fully condensed at 1900 °C. Since the density of CaB_6 is lower than the density of B_4C, the theoretical density of the samples decreases as the contribution rate increases.

The addition of 5wt% CaB_6 to B_4C caused a significant increase in bulk density. Compared to the B100 sample which was sintered without additives at the same temperature, the BC5 sample was improved densification. The decrease in open porosity supports this approach. The density measured in samples BC10 and BC15 and BC20 exceeded the calculated density. The reason for this is the Ti, Fe impurities from the raw materials and the Si_3N_4 ball and mill used during the homogenization process. The density of the impurities is higher than the density of the raw materials used. The presence of open porosity in the BC10, BC15 and BC20 samples indicates

that the samples are not fully densification, although the theoretical density is exceeded. When the results are analyzed in general, the CaB_6 additive resulted in a decrease in apparent porosity and theoretical density compared to the additive sample sintered at the same temperature.

Table 6.3 Open Porosity and Densities of Samples

Sample	Sintering Temperature (°C)	Theoretical Density (g/cm^3)	Bulk Density (g/cm^3)	Open Porosity (%)
B100	2050	2.5200	2.5146	0.105
B100	1900	2.5200	2.3879	4.5463
BC5	1900	2.5164	2.4942	1.0021
BC10	1900	2.5128	2.5298	0.0543
BC15	1900	2.5092	2.5160	0.2404
BC20	1900	2.5026	2.5245	0.0569

6.6 Phase Analysis

XRD analysis was performed for phase analysis of sintered samples. XRD patterns and resutls of the samples are given in Figure 6.11. Results show WC and SiC phases. There is no W or Si based impurty in the content of the raw materials. The ball and chamber used during homogenization are Si_3N_4, the hardness of which is lower than B_4C. During the process, Si_3N_4 contamination was introduced into the powder mixture due to the B_4C grains eroding the ball and the chamber. The impurty reacted with the carbon from the paper and mold during cooking to form the SiC compound. The decrease in hardness with the increase of CaB_6 ratio in the mixture led to a decrease in Si_3N_4 impurty. Therefore, SiC peaks are not observed in samples with high CaB_6 ratio (Figure 6.11-c-d-e).

Due to the hardness of B_4C and CaB_6 higher than WC, impurity contaminated from the ring mill during the milling of sintered samples. WC peaks are seen in all samples.

New phase formation is not seen in XRD results of the additive-free B100 sample, except for characteristic B_4C peaks. (Figure 6.11-a). CaB_6 peaks are seen in BC5 sample except B_4C (Figure 6.11-b). There is an increase in the intensity of the CaB_6 peaks due to the increase in the Ca ratio. (Figure 6.11-c-d-e). New phase formation is not seen in XRD results. Since the spark plasma sintering is carried out in a vacuum environment, oxidation does not occur except for the reactions originating from the oxygen in the sample. In addition, the rapid heating and cooling regime of the furnace prevents phase transformations. For this reason, no reaction and phase conversion between raw materials occurred during sintering.

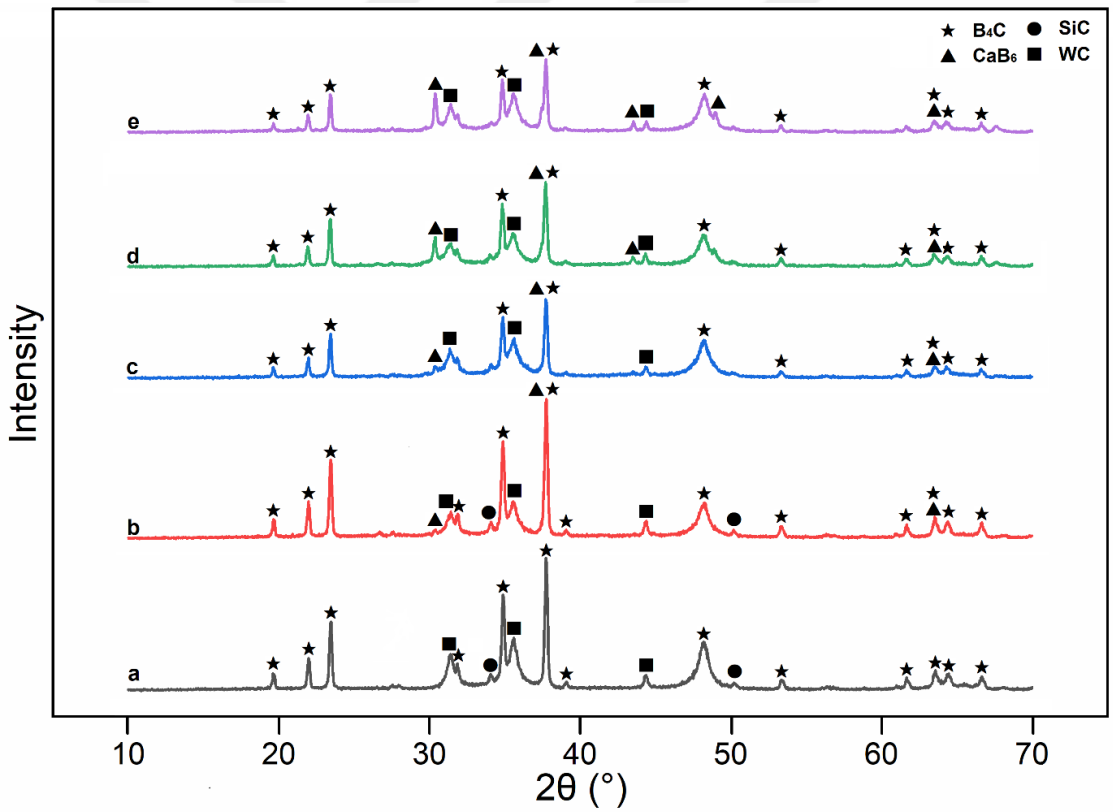


Figure 6.11 Sintering XRD Patterns of Sintered Samples a) B100 b) BC5 c) BC10 d) BC15 e) BC20

6.7 Microstructural Analysis

Microstructural analysis of samples cross-section surface was performed by scanning electron microscopy (SEM) and Energy-dispersive X-ray spectroscopy (EDS) after polishing. The reason for examining the sample section surface is that there is a high amount of C contamination on surfaces that from contact with mold and graphite paper.

Figure 6.12 shows the secondary electron image of the B100 sample without additives. Regions 1 and 2 show porosities. The bright white part in area 3 is the polishing solution. B_4C cannot be completely sintered at 1900 °C due to its strong covalent bonds. Porosities indicate that the sample did not complete sintering. The sintering graph and density/apparent porosity results support this view. Color differences on the sample surface.

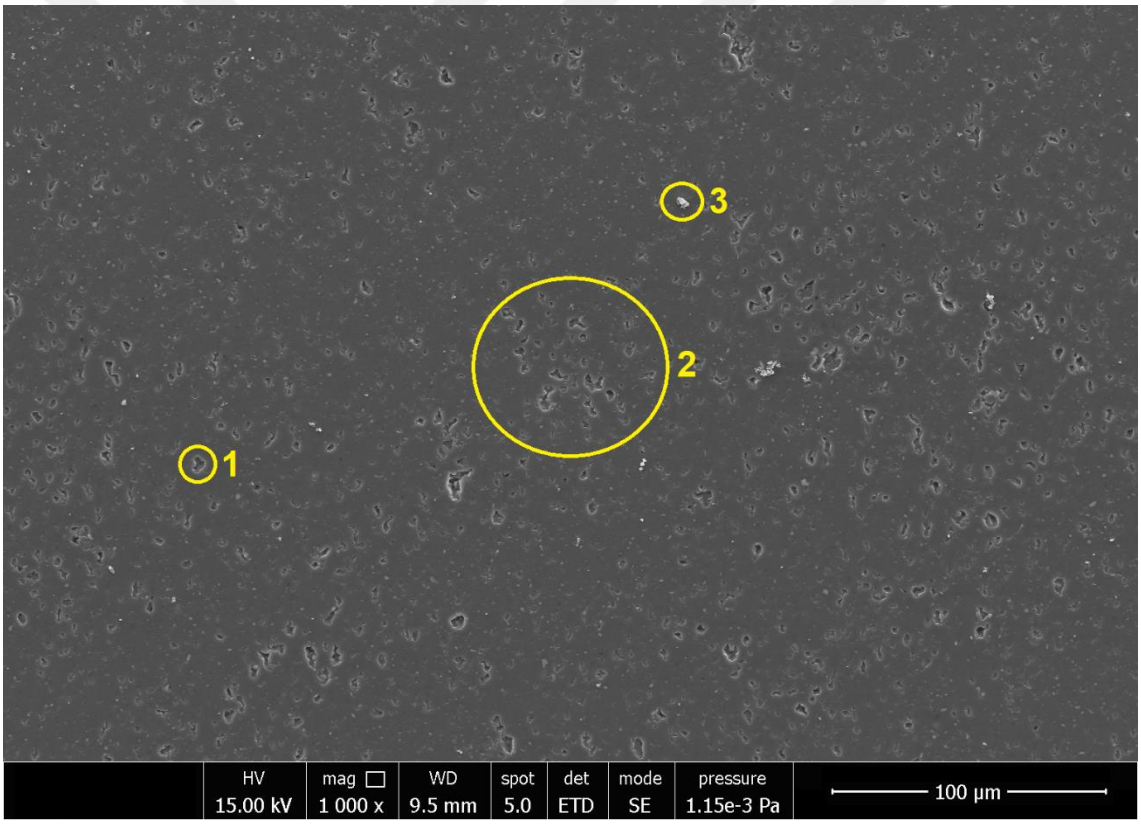


Figure 6.12 SEM Image of B100 Sample

In Figure 6.13, EDS analysis points are shown. EDS analysis was performed in Spot-1 to determine the content of bright regions or spots. It is observed that the bright regions are Ti, Si and N based impurities from the raw material and from the homogenization process. There are also no clear grain boundaries. The grain

boundaries disappeared during sintering. Since grain boundaries are not clear, grain size measurement could not be made. However, due to the low sintering temperature, porosities are not filled and still exist. The distribution and shape of porosities are not homogeneous. The impurities contained in the raw material may have caused this irregularities.

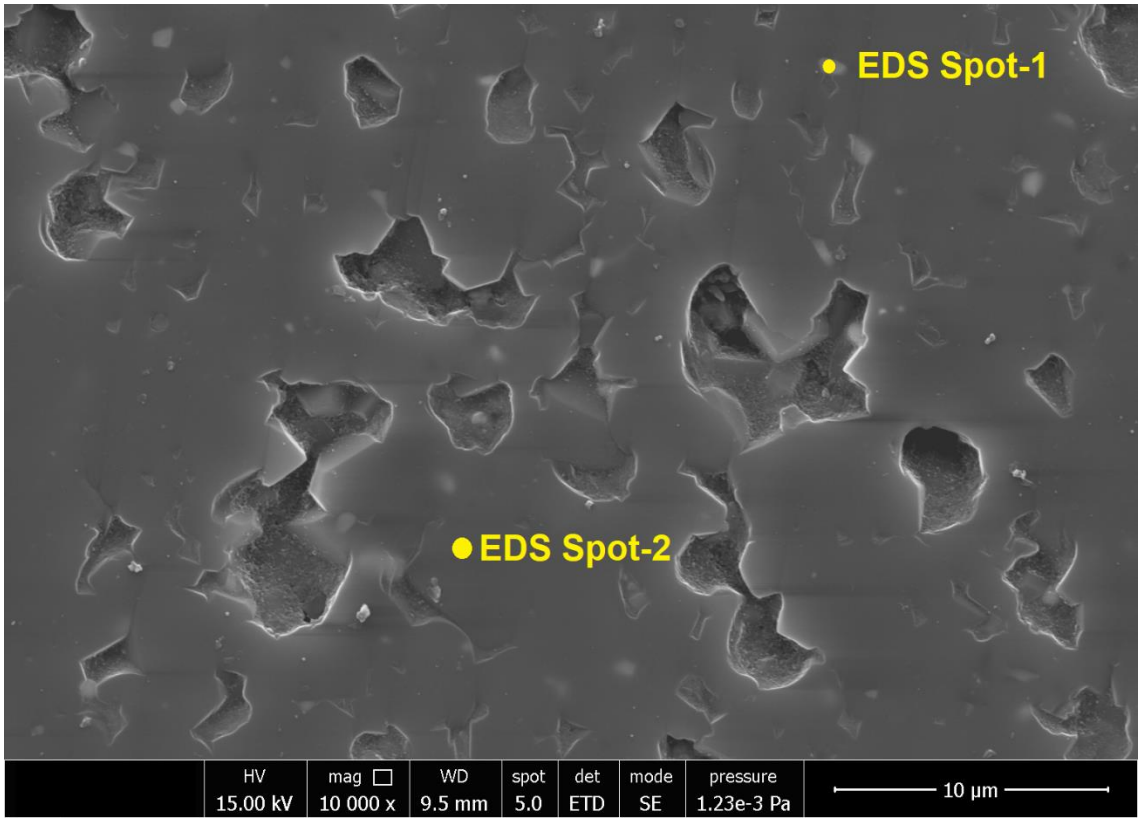


Figure 6.13 SEM Image and EDS Spots of B100 Sample

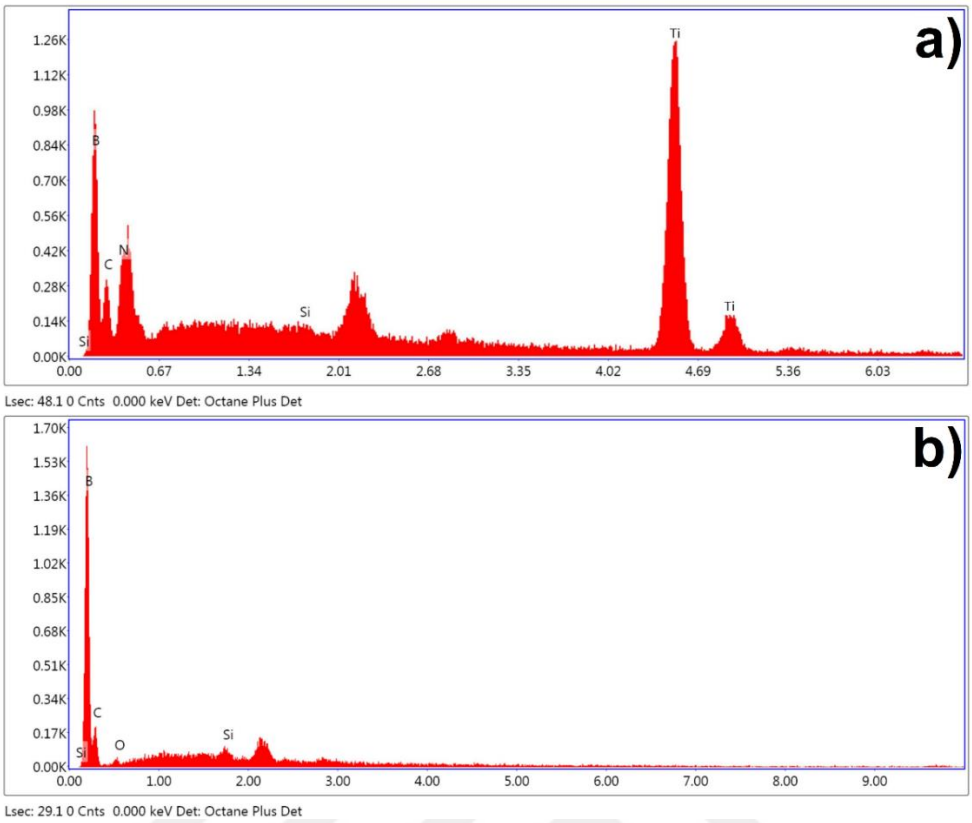


Figure 6.14 EDS Analysis of B100 Sample

Figure 6.15 shows an electron microscope image of the BC5 sample with 5 wt% CaB_6 added. In Figure 6.16, EDS points are given. The white areas appear to be CaB_6 and impurities. In the B_4C matrix, Si, which contaminated during homogenization and which reacts to the carbon, forms SiC. It is seen that the secondary phase, CaB_6, is homogeneously distributed in the structure. In open porosity measurement, it was determined that the amount of open porosity decreased and density increased in BC5 sample compared to monolithic B_4C. The decrease in porosity in SEM images supports the decrease in open porosity and increase in density.

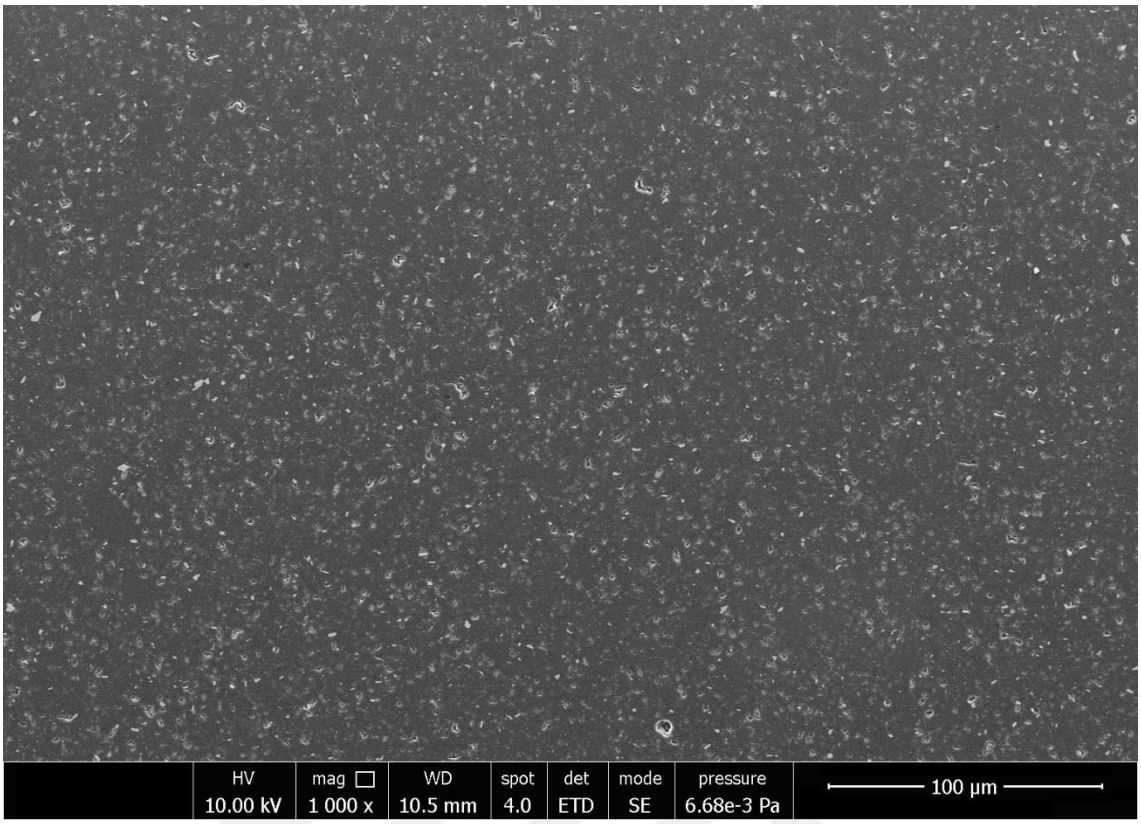


Figure 6.15 SEM-Secondary Electron Image of BC5 Sample

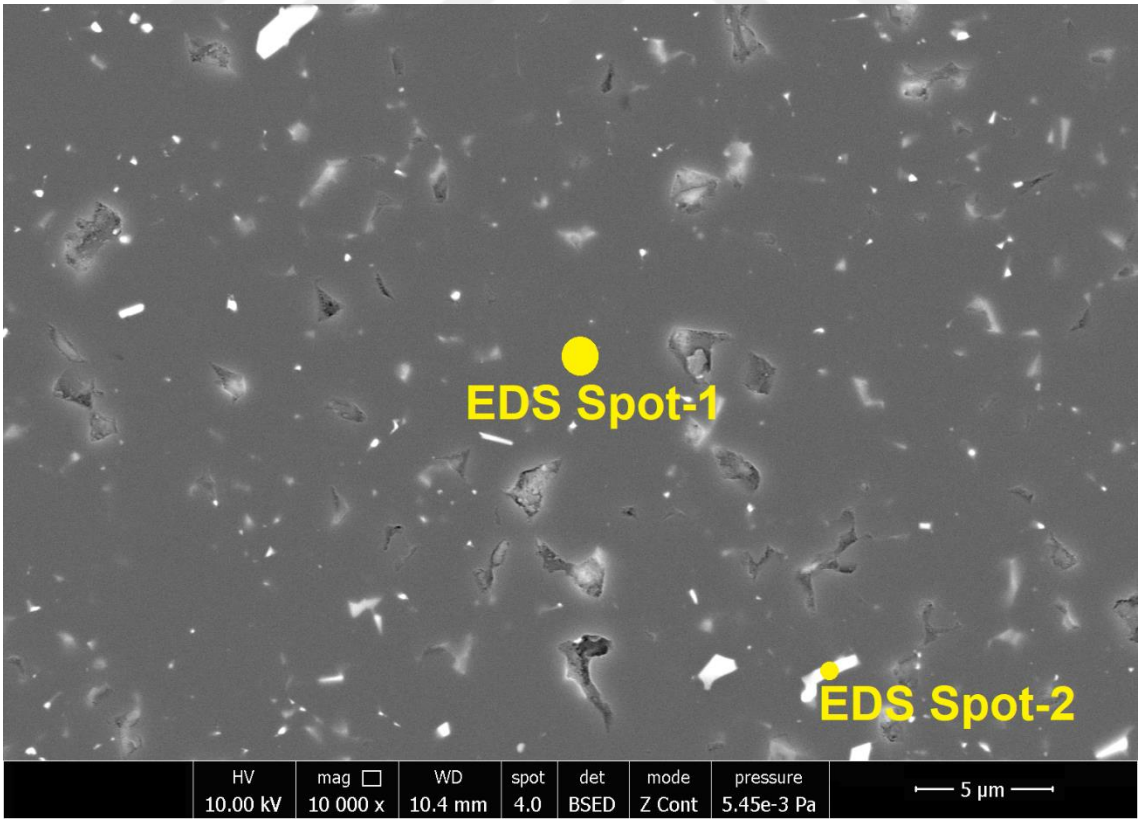


Figure 6.16 SEM Image and EDS Spots of BC5 Sample

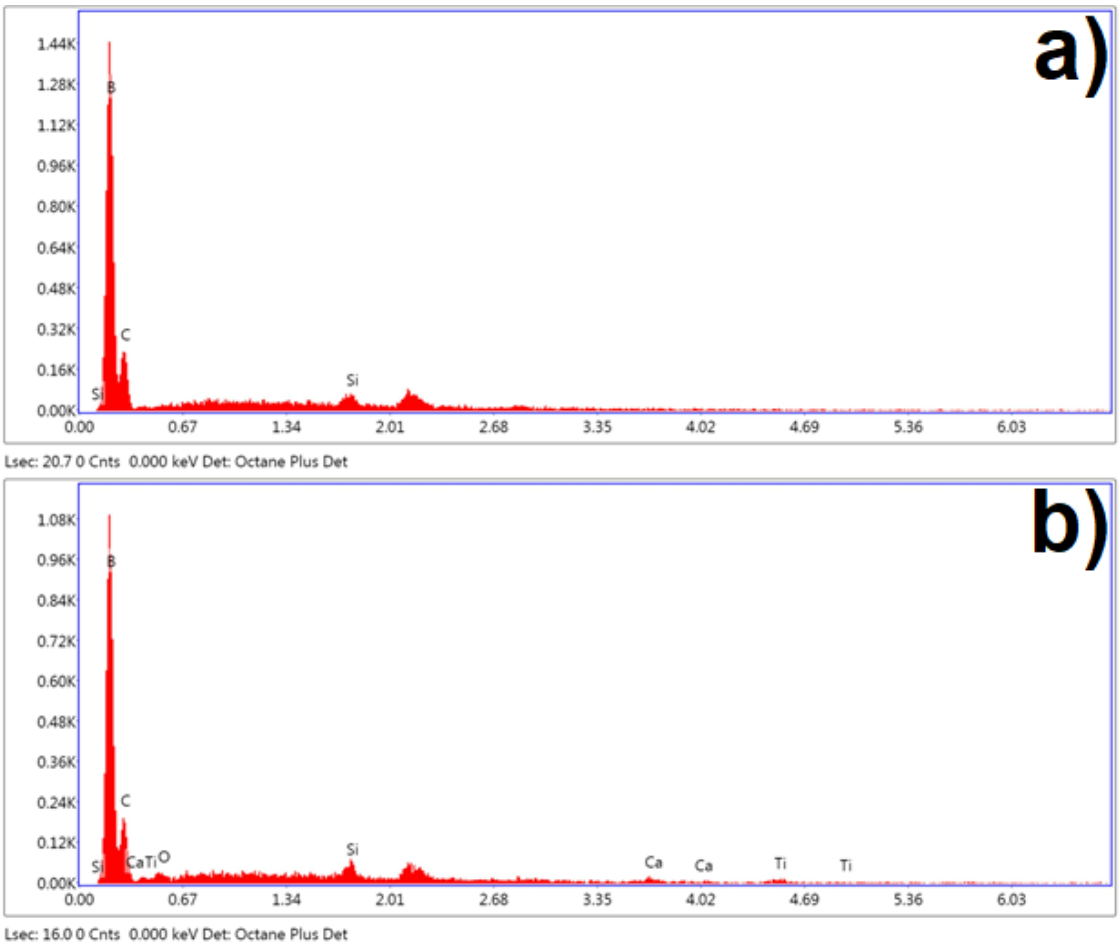


Figure 6.17 EDS Analysis of BC5 Sample

Table 6.4 EDS Analysis of BC5 Sample

EDS Spot-1		**EDS Spot-2**	
Elemental	**Weight %**	**Elemental**	**Weight %**
B K	76.38	B K	75.29
C K	23.07	C K	22.85
Si K	0.55	O K	0.23
		Si K	0.61
		Ca K	0.40
		Ti K	0.61

In the Figure 6.18, back scattered electron image of BC10 sample is given. Similar to the BC5 sample, a homogeneous secondary phase distribution is observed. The decrease in porosity is consistent with the density and open porosity results. Mechanical properties of CaB_6 are lower than B_4C. Therefore, CaB_6 grains were damaged during sample polishing, as in the first region mentioned in Figure 6.19. Chip-off occurred in the 2nd region. Another reason for chip off may be the thermal expansion coefficient difference. Unlike porosities, chip-off regions have an angular structure. On the other hand, the regions containing porosity have soft edges originating from the start of granulation.

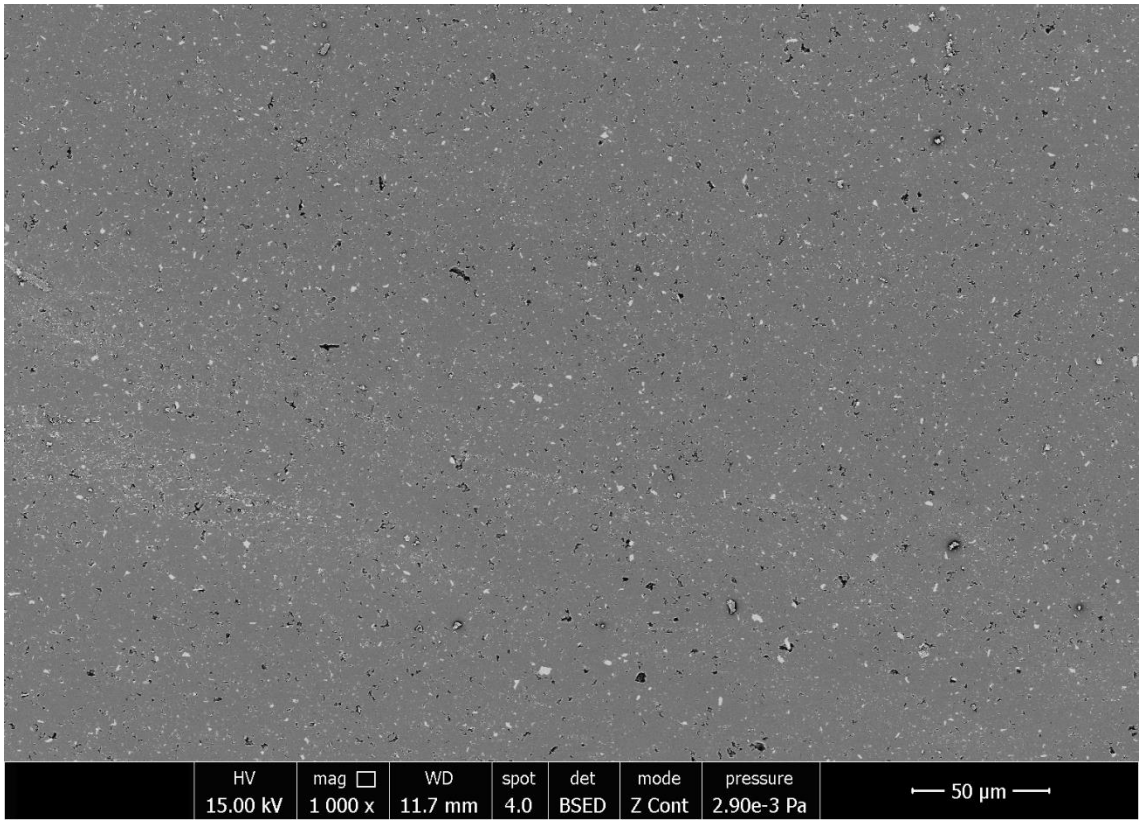


Figure 6.18 SEM-Back Scattered Electron Image of BC10 Sample (1000x)

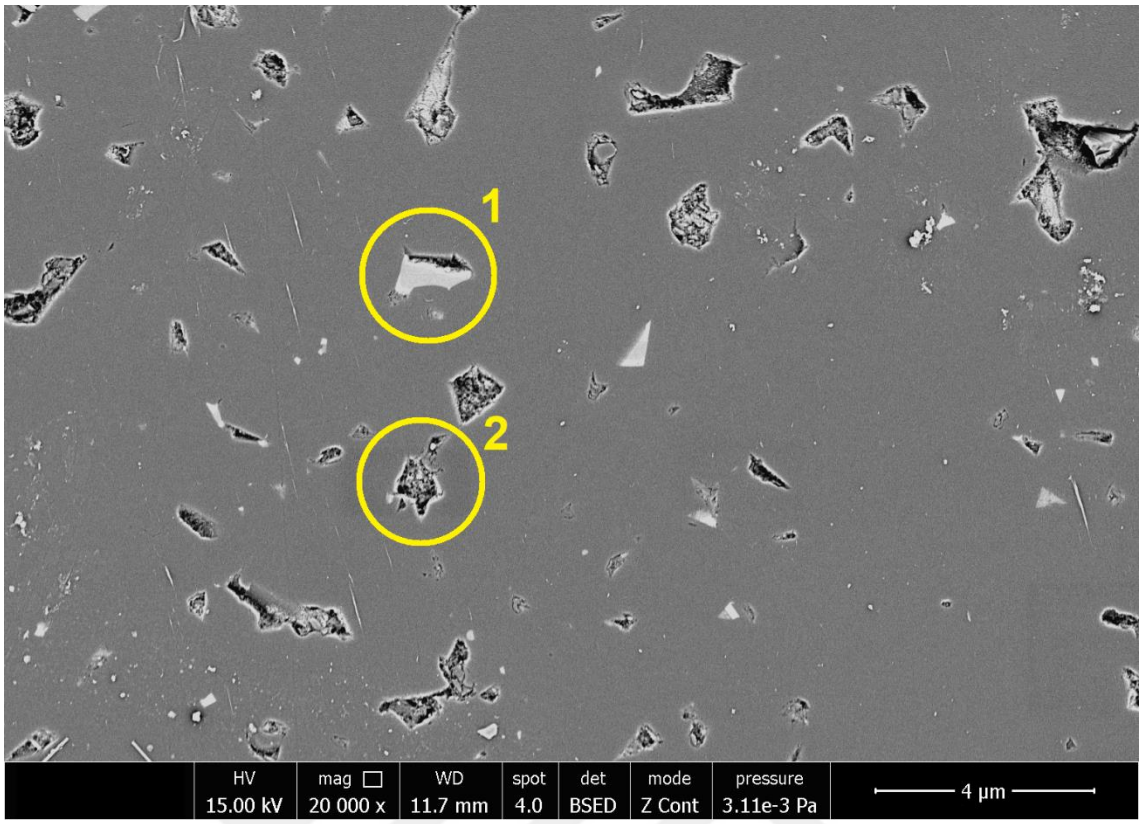


Figure 6.19 SEM-Back Scattered Electron Image of BC10 Sample (20000x)

Figure 6.20 shown BSE image of BC15 sample. In the BC15 sample, the CaB_6 phase appears to have a heterogeneous distribution compared to other samples. Large CaB_6 grains appear to be clustered. In the parts with small size CaB_6 grains, an increase in porosity and chip-off amounts are observed. The decrease in density and increase in open porosity ratio supports the increase in porosity formation. Heterogeneous grain distribution may result from sample preparation processes.

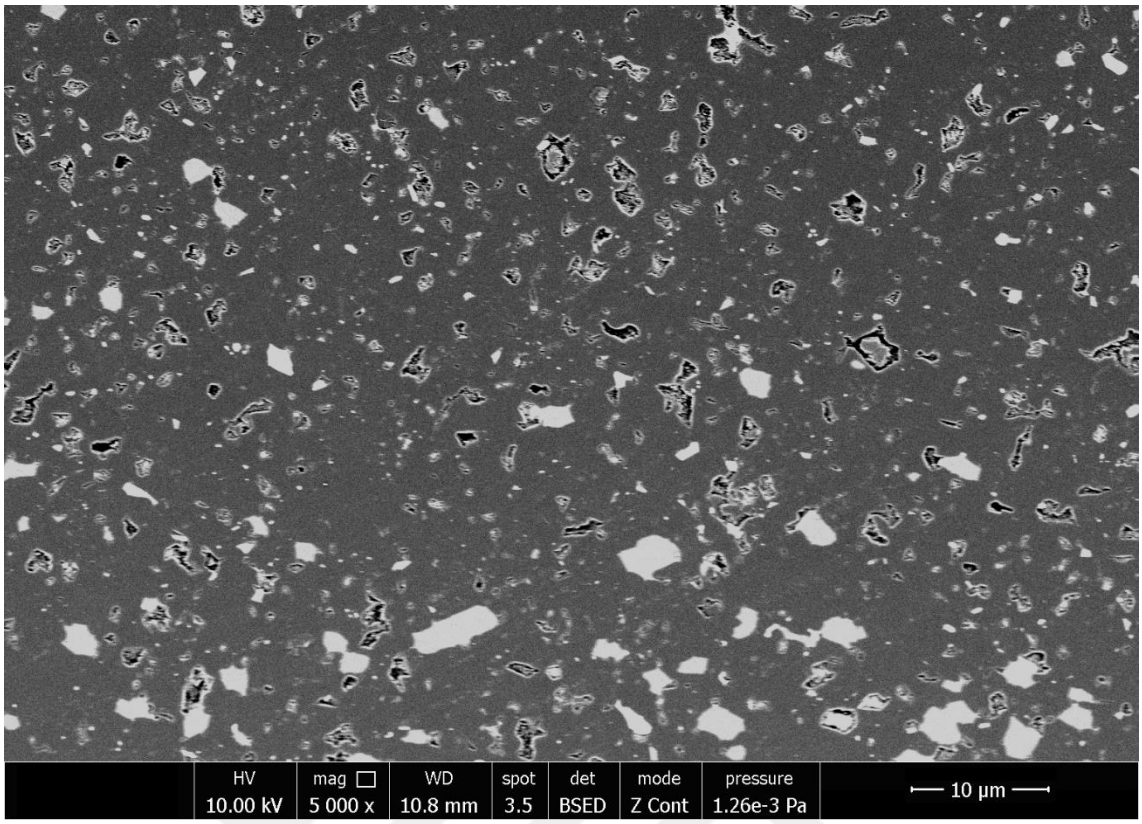


Figure 6.20 SEM-Back Scattered Electron Image of BC15 Sample (5000x)

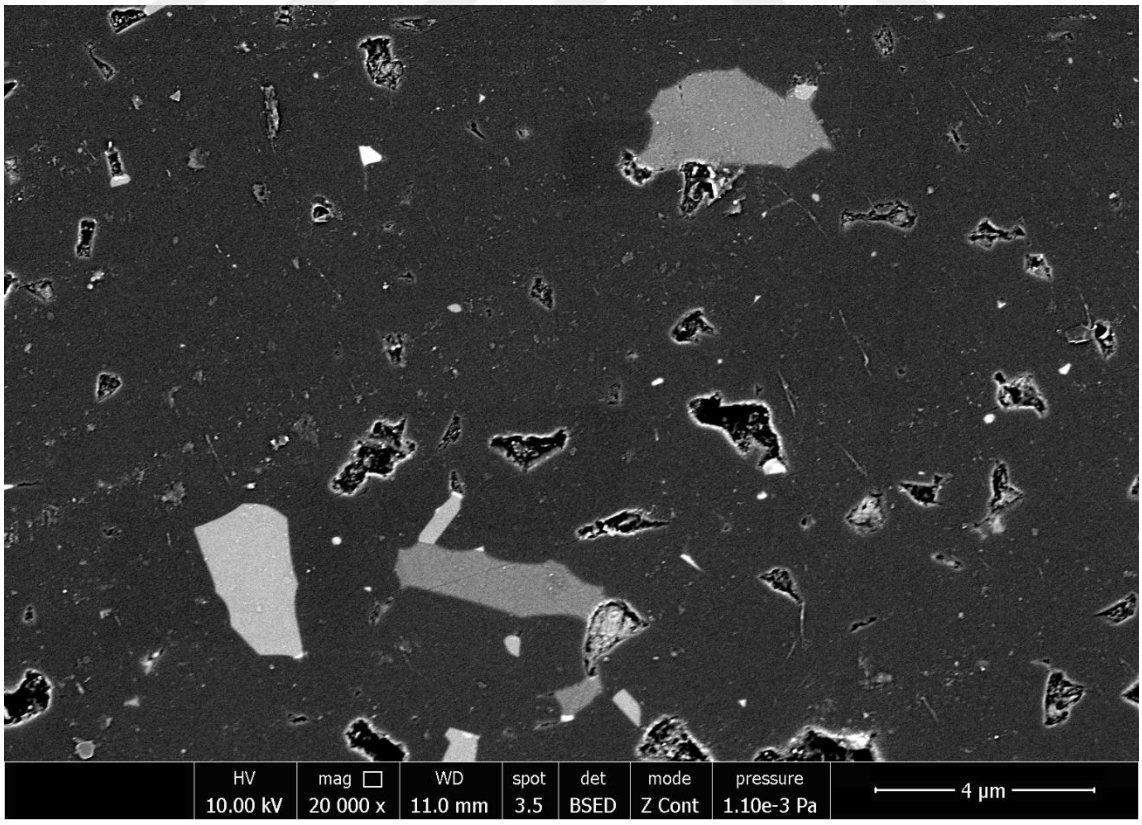


Figure 6.21 SEM-Back Scattered Electron Image of BC15 Sample (20000x)

In Figure 6.22, EDS points of B20 sample are given. The white areas shown as EDS Area-1 appear to be CaB_6 grains. The part marked as EDS Area-2 (Figure 6.23) is the B_4C matrix. Impurities from raw materials are not seen at both points. The region seen in EDS Spot-2 is the point where the raw materials and the impurities coming from the grinding process are collected. There is a low amount of CaB_6 in the region. The SiC seen in the XRD results is seen at this point. Fractures appear in large CaB_6 grains. These breaks may be the reason for the chip-off defect that started to appear from the BC10 sample.

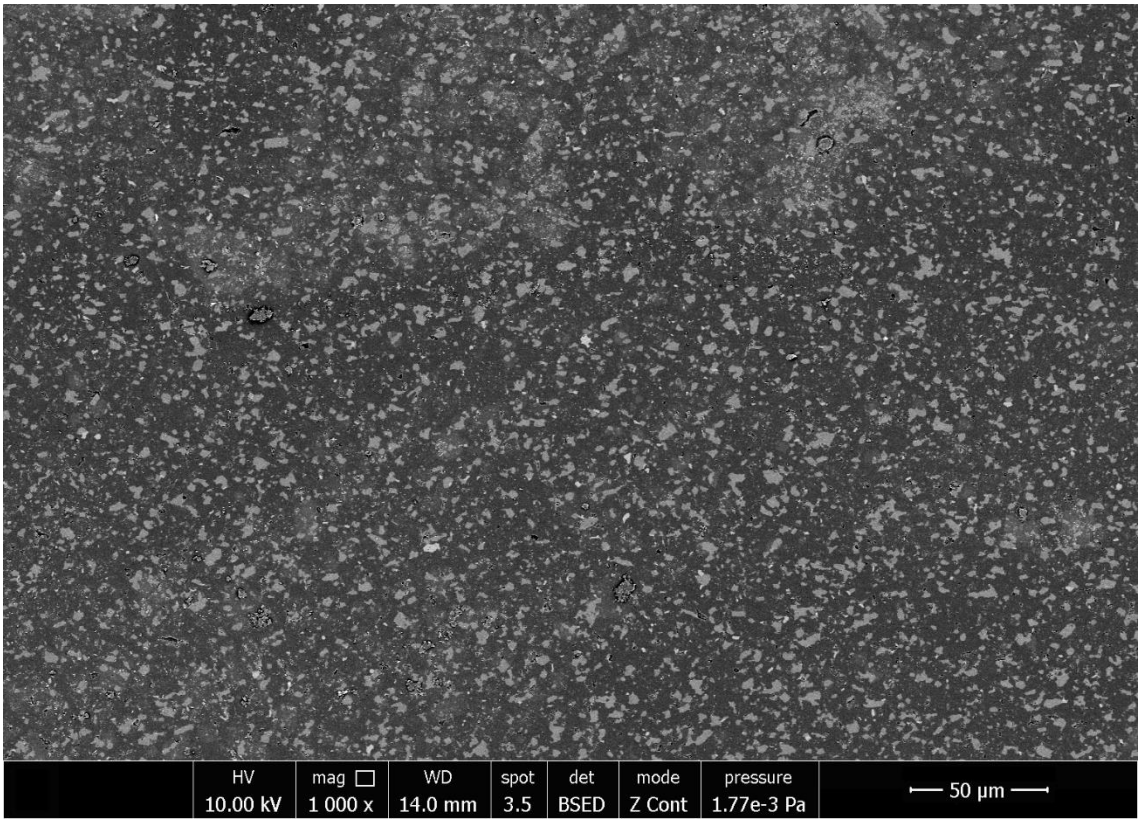


Figure 6.22 SEM-Back Scattered Electron Image of BC20 Sample (20000x)

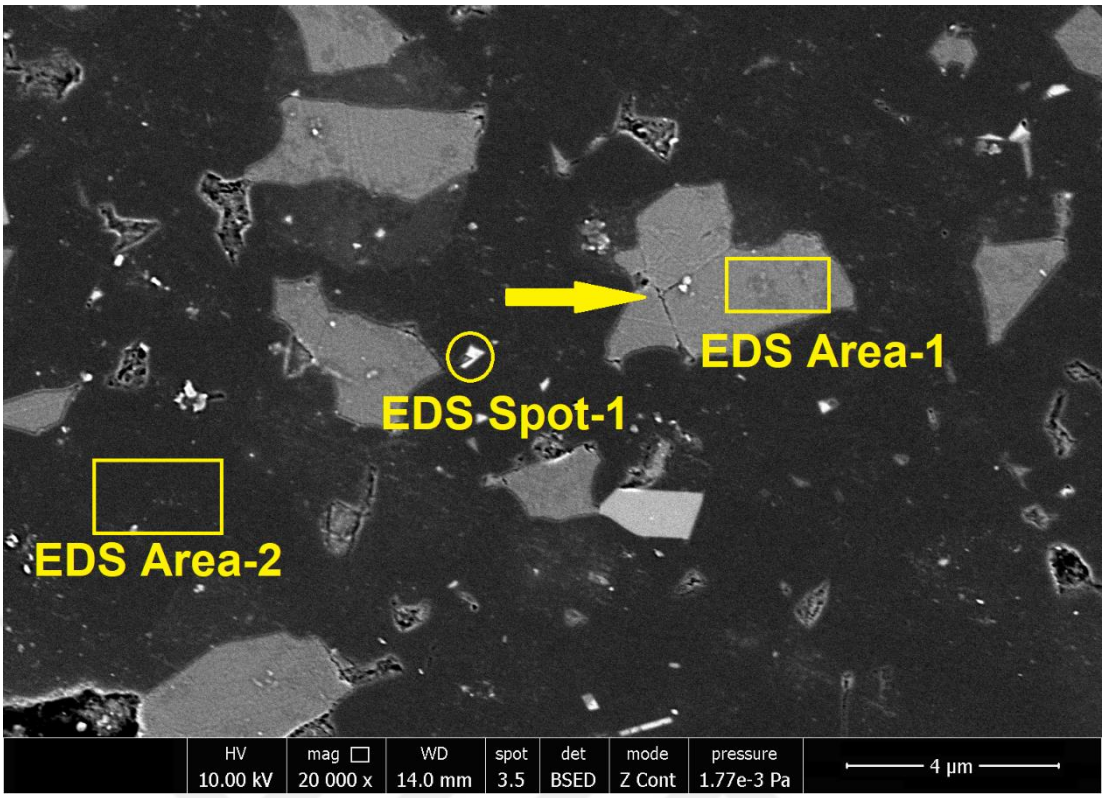


Figure 6.23 SEM Image and EDS Spots of BC20 Sample

Table 6.5 EDS Analysis of B20 Sample

EDS Area-1		EDS Area-2		EDS Spot-1	
Elemental	Weight %	Elemental	Weight %	Elemental	Weight %
B K	68.52	B K	76.60	B K	12.56
C K	8.92	C K	23.40	C K	16.9
O K	0.28			Si K	7,73
Ca K	22.28			Ca K	3.30
				Ti K	59.51

6.8 Hardness and Fracture Toughness

The hardness and toughness values of the sintered samples were measured to investigate the effect of the addition of CaB_6 to the B_4C phase on the mechanical properties. Measured values are given in the Figure 6.24. For measurement accuracy, three measurements were taken from each sample, and the mean and standard deviations were calculated.

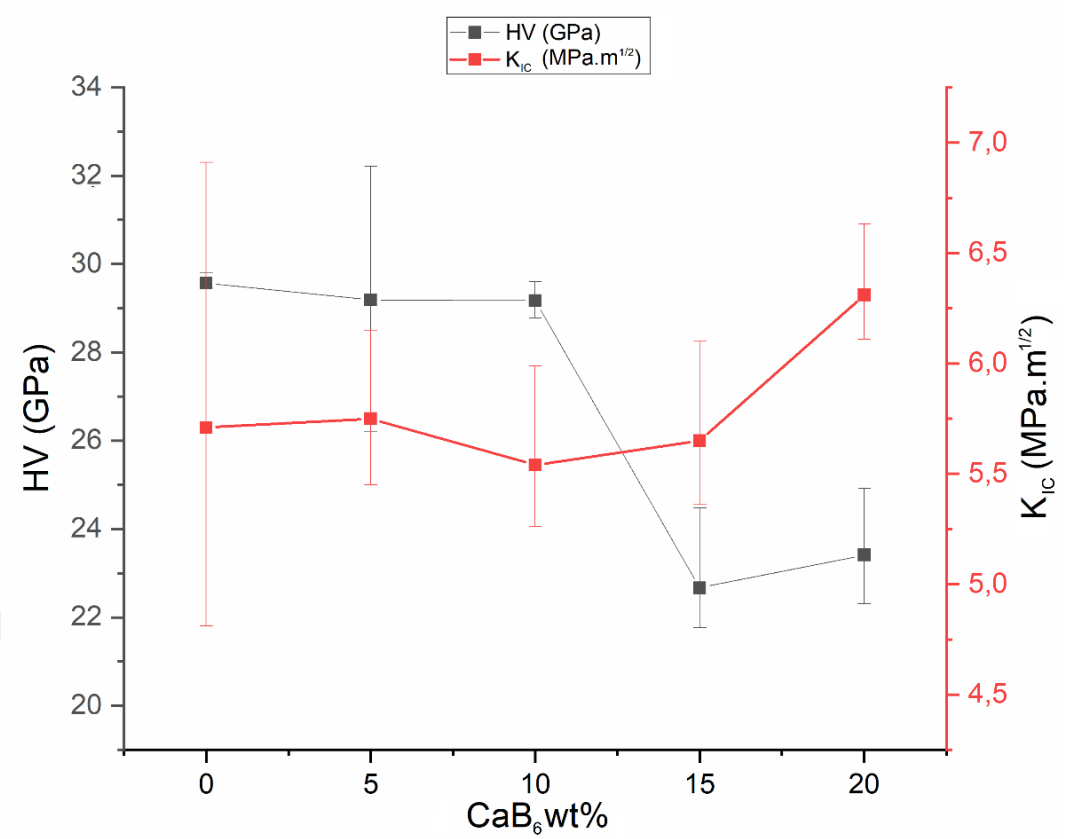


Figure 6.24 Effect of CaB6 Ratio on Fracture Toughness and Hardness

The hardness value of the additive-free B100 sample is below the B_4C hardness value known in the literature. This is because the sample is not fully sintered. Porosity in the structure caused low hardness value. The hardness value of the sample is 29.57 GPa HV. Since the hardness of the CaB_6 phase is low compared to the B_4C matrix, the hardness values decrease due to the addition of CaB_6. With the addition of 5wt% CaB_6, the hardness value decreased by 0.38 points and HV was measured as 29.19 GPa HV. However, the standard deviation of the measurements is high compared to the B100 sample. This can be explained by the fact that the measuring points are on or near the CaB_6 phase. The drop in hardness continued with the addition of 10wt% CaB_6. Hardness value decreased to 29.17 GPa HV. However, with increasing CaB_6 ratio, the probability of measuring points being above or near the secondary surplus increased, thereby reducing standard deviation. BC15 was the sample with the highest porosity among the additive samples with the addition of 15wt% CaB_6. The hardness value also parallels this. The hardness of the BC15 sample with the lowest hardness value is 22.67 GPa HV.

The BC20 sample has a hardness of 0.75 points higher than 15wt%, while still low compared to other samples. BC20 samples hardness is 23.41 GPa HV. In general, the hardness value decreases with the addition of CaB_6. With the increase in CaB_6 ratio, the amount of decrease in hardness increased.

There is a relationship between fracture toughness and hardness. Fracture toughness of high hardness materials is generally low. In B_4C, strong covalent bonds that provide rigidity ensure low fracture toughness. Fracture toughness of CaB_6 is higher than B_4C. This feature affected the fracture toughness of the samples. The fracture toughness of the monolithic B_4C sample was measured as 5.71 $MPa.m^{1/2}$. Although this value is above the monolithic B_4C value known in the literature, it can be explained with low hardness. Fracture toughnesses were measured as 5.75 $MPa.m^{1/2}$, 5.54 $MPa.m^{1/2}$ and 5,65 $MPa.m^{1/2}$ in BC5, BC10 and BC15 samples, respectively. The fracture toughness of the BC20 sample containing 20wt% CaB_6 increasing by 0.6 points compared to the monolithic B_4C, was measured as 6.31 $MPa.m^{1/2}$.

Irregularity in mechanical properties is similar to B_4C-CaB_6 studies in the literature. The reason for this irregularity may be due to the difference of thermal expansion coefficients. The difference between the coefficients of thermal expansion lowers the hardness by causing residual stress during the cooling. But accordingly, an improvement in fracture toughness is observed. The addition of CaB_6 to the B_4C matrix gave similar results with this approach.

6.9 Conclusion and Recommendation

In this study, B_4C- CaB_6 composites containing 5 wt%, 10 wt%, 15 wt% and 20 wt% CaB_6 are sintered by Spark Plasma Sintering method. Sintering parameters are 1900 °C under vacuum, 30 MPa pressure. Sintering behaviors of the samples were examined on the temperature-time-shrinkage graph. Density and apparent porosity values of the samples were measured. XRD method was used to determine the phase transformations that may occur during sintering. Microstructures of sintered samples were examined by SEM-EDS method. In order to examine the effect of CaB_6 additive ratio on mechanical properties, hardness and fracture toughness values were measured.

With the addition of CaB_6 in the mixture, the sintering initial temperatures decreased. The sinterability of CaB_6 is better compared to B_4C. This is because his Ca-B bond is weaker than the B-C bond. Easier sintering of CaB_6 affected the sintering behavior of the B_4C-CaB_6 composite. The sample containing 20 wt% CaB_6 started to be sintered at a temperature of 1030 °C, 330 °C lower than monolithic B_4C. Sintering started at a low temperature caused sintering to be completed faster.

The relative density of the monolithic B_4C sample sintered at 1900 °C was 94.75%. The low density of CaB_6 compared to B_4C caused the theoretical density to be low. The relative density increased to 99.11% with the addition of 5wt% CaB_6. The relative density with the addition of 5 wt%, 10 wt% and 15 wt% CaB_6 is 100.67, 100.27 and 100.87, respectively. Density value, higher than the theoretical value, is caused by the impurities in the raw material.

New phase formation is not seen in XRD phase analysis. It was found that no reaction occurred between B_4C and CaB_6 during sintering.

When microstructures are examined, it is seen that the CaB_6 additive is distributed homogeneously in general. The decrease in open porosity also reduced the porosity in the microstructure. Grain boundaries have disappeared. This shows that sintering is easier. However, there are porosities indicating that sintering is not fully completed in the samples.

The addition of CaB_6 negatively affected the hardness value of B_4C. With the increase in CaB_6 ratio, the decrease in hardness value increased. The hardness value was measured as 23.41 GPa with the addition of 20wt% CaB_6, decreasing by 6.16 points compared to monolithic B_4C.

Fracture toughness increased on the contrary to hardness measurements. An increase in fracture toughness was measured by the addition of CaB_6. The fracture toughness of monolithic B_4C increased from 5.71 MPa.m½ to 6.31 MPa.m½ with the addition of 20wt% CaB_6.

During the study, it was observed that the ability of B_4C to be sintered increased with the addition of CaB_6. It was analyzed that no reaction occurred between B_4C

and CaB_6. The optimum result in terms of sinterability-mechanical properties was the addition of 20% CaB_6.

In future studies, ceramic composites with a triple phase diagram can be developed by adding other additives such as TiB_2, SiC, TiC in addition to the addition of CaB_6 sinter additive. The third phase addition can help improve mechanical properties.

REFERENCES

[1] S. Mathur and M. Driess, "From Metal–Organic Precursors to Functional Ceramics and Related Nanoscale Materials," in *Comprehensive Organometallic Chemistry III*, no. 2, Elsevier, 2007, pp. 35–70.

[2] N. Hosmane, *Boron science: New technologies and applications*. CRC Press, 2011.

[3] S. Mondal and A. K. Banthia, "Low-temperature synthetic route for boron carbide," *J. Eur. Ceram. Soc.*, vol. 25, no. 2–3, pp. 287–291, Jan. 2005, doi: 10.1016/j.jeurceramsoc.2004.08.011.

[4] I. G. Crouch, G. V. Franks, C. Tallon, S. Thomas, and M. Naebe, "Glasses and ceramics," in *The Science of Armour Materials*, Elsevier, 2017, pp. 331–393.

[5] H.-W. Kim, Y.-H. Koh, and H.-E. Kim, "Densification and Mechanical Properties of B4C with Al2O3 as a Sintering Aid," *J. Am. Ceram. Soc.*, vol. 83, no. 11, pp. 2863–2865, Dec. 2004, doi: 10.1111/j.1151-2916.2000.tb01647.x.

[6] C. J. ENGBERG and E. H. ZEHMS, "Thermal Expansion of Al2O3, BeO, MgO, B4C, SiC, and TiC Above 1000oC.," *J. Am. Ceram. Soc.*, vol. 42, no. 6, pp. 300–305, Jun. 1959, doi: 10.1111/j.1151-2916.1959.tb12958.x.

[7] A. G. Evans, "Perspective on the Development of High-Toughness Ceramics," *J. Am. Ceram. Soc.*, vol. 73, no. 2, pp. 187–206, Feb. 1990, doi: 10.1111/j.1151-2916.1990.tb06493.x.

[8] M. v. Stackelberg and F. Neumann, "Die Kristallstruktur der Boride der Zusammensetzung MeB6," *Zeitschrift für Phys. Chemie*, vol. 19B, no. 1, pp. 314–320, Jan. 1932, doi: 10.1515/zpch-1932-1932.

[9] S. Shah and A. N. Kolmogorov, "Stability and superconductivity of Ca-B phases at ambient and high pressure," vol. 2, pp. 1–12, Jul. 2013, doi: 10.1103/PhysRevB.88.014107.

[10] I. Matkovich and E. Board, *Boron and Refractory Borides*. Berlin, Heidelberg: Springer Berlin Heidelberg, 1977.

[11] M. Kakiage, S. Shiomi, I. Yanase, and H. Kobayashi, "Low-Temperature Synthesis of Calcium Hexaboride Powder via Transient Boron Carbide Formation," *J. Am. Ceram. Soc.*, vol. 98, no. 9, pp. 2724–2727, Sep. 2015, doi: 10.1111/jace.13771.

[12] Z. Lin, M. Guanghui, and Y. Huashun, "Reaction mechanism and size control of CaB6 micron powder synthesized by the boroncarbide method," *Ceram. Int.*, vol. 35, no. 8, pp. 3533–3536, Dec. 2009, doi: 10.1016/j.ceramint.2009.05.032.

[13] T. T. Xu, J. Zheng, A. W. Nicholls, S. Stankovich, R. D. Piner, and R. S. Ruoff, "Single-Crystal Calcium Hexaboride Nanowires: Synthesis and Characterization," *Nano Lett.*, vol. 4, no. 10, pp. 2051–2055, Oct. 2004, doi:

10.1021/nl0486620.

[14] J. Matsushita and S. Komarneni, “High temperature oxidation behavior of CaB6 sintered body,” *J. Mater. Sci.*, vol. 4, pp. 3043–3046, 1999, doi: 10.1023/A:1004628327799.

[15] S. . Zheng, G. . Min, Z. . Zou, and C. Tatsuyama, “High temperature oxidation of calcium hexaboride powders,” *Mater. Lett.*, vol. 58, no. 21, pp. 2586–2589, Aug. 2004, doi: 10.1016/j.matlet.2004.02.053.

[16] B. A. Galanov *et al.*, “Penetration Resistance of B4C-CaB6 Based Light-weight Armor Materials,” *Procedia Eng.*, vol. 58, pp. 328–337, 2013, doi: 10.1016/j.proeng.2013.05.037.

[17] Y. Qiao, L. Qu, X. Zhang, and H. Zhang, “Boron carbide composite ceramic preparation and corrosion behavior in simulated seawater,” *Ceram. Int.*, vol. 41, no. 3, pp. 5026–5031, Apr. 2015, doi: 10.1016/j.ceramint.2014.12.070.

[18] T. Ogitsu, F. Gygi, J. Reed, Y. Motome, E. Schwegler, and G. Galli, “Imperfect Crystal and Unusual Semiconductor: Boron, a Frustrated Element,” *J. Am. Chem. Soc.*, vol. 131, no. 5, pp. 1903–1909, Feb. 2009, doi: 10.1021/ja807622w.

[19] M. L. Mckee and T. F. Element, *Boron*, vol. 20. Cham: Springer International Publishing, 2015.

[20] D. M. Schubert, “Boron: Inorganic Chemistry,” in *Encyclopedia of Inorganic and Bioinorganic Chemistry*, Wiley, 2019, pp. 1–21.

[21] K. Yünlü, *Bor*. Ankara: Boren, 2016.

[22] V. M. Shorrocks and M. Bureau, “The occurrence and correction of boron deficiency,” *Plant Soil*, pp. 121–148, 1997, doi: 10.1023/A:1004216126069.

[23] M. S. Celik, H. A. Uzunoglu, and F. Arslan, “Decrepitation properties of some boron minerals,” *Powder Technol.*, vol. 79, no. 2, pp. 167–172, May 1994, doi: 10.1016/0032-5910(94)02811-7.

[24] Y. Kar, N. Şen, and A. Demirbaş, “Boron Minerals in Turkey, Their Application Areas and Importance for the Country’s Economy,” *Miner. Energy - Raw Mater. Rep.*, vol. 20, no. 3–4, pp. 2–10, Jan. 2006, doi: 10.1080/14041040500504293.

[25] J. L. PARKS and M. EDWARDS, “Boron in the Environment,” *Crit. Rev. Environ. Sci. Technol.*, vol. 35, no. 2, pp. 81–114, Mar. 2005, doi: 10.1080/10643380590900200.

[26] H. Hale, “A Textbook of Inorganic Chemistry. Third edition (Partington, J. R.),” *J. Chem. Educ.*, vol. 8, no. 12, p. 2474, Dec. 1931, doi: 10.1021/ed008p2474.1.

[27] A. E. TUTTON, “The Properties of Amorphous Boron,” *Nature*, vol. 45, no. 1170, pp. 522–523, Mar. 1892, doi: 10.1038/045522a0.

[28] S. Chandra, *Comprehensive Inorganic Chemistry*. New Age International, 2005.

[29] “Bor Elementi.” http://www.etimaden.gov.tr/bor-elementi (accessed May 28, 2020).

[30] X. Sun *et al.*, "Two-Dimensional Boron Crystals: Structural Stability, Tunable Properties, Fabrications and Applications," *Adv. Funct. Mater.*, vol. 27, no. 19, p. 1603300, May 2017, doi: 10.1002/adfm.201603300.

[31] Kirk-Othmer, *Encyclopedia of Chemical Technology*. Wiley, 2000.

[32] "Boron Global Industry, Markets & Outlook," 2015.

[33] D. M. Schubert, "Boric Oxide, Boric Acid, and Borates," in *Ullmann's Encyclopedia of Industrial Chemistry*, Weinheim, Germany: Wiley-VCH Verlag GmbH & Co. KGaA, 2015, pp. 1–32.

[34] "Boron Products Schematic." https://www.boren.gov.tr/pages/boron-products-schematic/114 (accessed May 28, 2020).

[35] V. Domnich, S. Reynaud, R. A. Haber, and M. Chhowalla, "Boron carbide: Structure, properties, and stability under stress," *J. Am. Ceram. Soc.*, vol. 94, no. 11, pp. 3605–3628, 2011, doi: 10.1111/j.1551-2916.2011.04865.x.

[36] A. K. Suri, C. Subramanian, J. K. Sonber, and T. S. R. C. Murthy, "Synthesis and consolidation of boron carbide: a review," *Int. Mater. Rev.*, vol. 55, no. 1, pp. 4–40, Jan. 2010, doi: 10.1179/095066009X12506721665211.

[37] Z. Han, G. Li, J. Tian, and M. Gu, "Microstructure and mechanical properties of boron carbide thin films," *Mater. Lett.*, vol. 57, no. 4, pp. 899–903, 2002, doi: 10.1016/S0167-577X(02)00892-3.

[38] M. Beauvy, "Stoichiometric limits of carbon-rich boron carbide phases," *J. Less-Common Met.*, vol. 90, no. 2, pp. 169–175, 1983, doi: 10.1016/0022-5088(83)90067-X.

[39] J. Greim and K. A. Schwetz, "Boron Carbide, Boron Nitride, and Metal Borides," in *Ullmann's Encyclopedia of Industrial Chemistry*, vol. 100 C, Weinheim, Germany: Wiley-VCH Verlag GmbH & Co. KGaA, 2006, pp. 121–145.

[40] A. K. Khanra, "Production of boron carbide powder by carbothermal synthesis of gel material," *Bull. Mater. Sci.*, vol. 30, no. 2, pp. 93–96, Apr. 2007, doi: 10.1007/s12034-007-0016-7.

[41] D. E. Taylor, J. W. McCauley, and T. W. Wright, "The effects of stoichiometry on the mechanical properties of icosahedral boron carbide under loading," *J. Phys. Condens. Matter*, vol. 24, no. 50, p. 505402, Dec. 2012, doi: 10.1088/0953-8984/24/50/505402.

[42] M. Bouchacourt and F. Thevenot, "The properties and structure of the boron carbide phase," *J. Less-Common Met.*, vol. 82, no. C, pp. 227–235, 1981, doi: 10.1016/0022-5088(81)90223-X.

[43] I. Gunjishima, T. Akashi, and T. Goto, "Characterization of directionally solidified B4C-TiB2 composites prepared by a floating zone method," *Mater. Trans.*, vol. 43, no. 4, pp. 712–720, 2002, doi: 10.2320/matertrans.43.712.

[44] M. Bouchacourt and F. Thevenot, "The melting of boron carbide and the homogeneity range of the boron carbide phase," *J. Less-Common Met.*, vol. 67, no. 2, pp. 327–331, 1979, doi: 10.1016/0022-5088(79)90007-9.

[45] H. K. Clark and J. L. Hoard, "The Crystal Structure of Boron Carbide," *J. Am. Chem. Soc.*, vol. 65, no. 11, pp. 2115–2119, Nov. 1943, doi: 10.1021/ja01251a026.

[46] H. L. Yakel, "The crystal structure of a boron-rich boron carbide," *Acta Crystallogr. Sect. B Struct. Crystallogr. Cryst. Chem.*, vol. 31, no. 7, pp. 1797–1806, Jul. 1975, doi: 10.1107/S0567740875006267.

[47] B. Çiçek and O. Karaahmet, *Bor Karbür ve Düşük Sıcaklık Bor Karbür Sentezleme Yöntemleri*. Ankara: Nobel Akademik Yayıncılık, 2018.

[48] L. Vargas-Gonzalez, R. F. Speyer, and J. Campbell, "Flexural Strength, Fracture Toughness, and Hardness of Silicon Carbide and Boron Carbide Armor Ceramics," *Int. J. Appl. Ceram. Technol.*, vol. 7, no. 5, pp. 643–651, Feb. 2010, doi: 10.1111/j.1744-7402.2010.02501.x.

[49] H. Lee and R. F. Speyer, "Hardness and Fracture Toughness of Pressureless-Sintered Boron Carbide (B4C)," *J. Am. Ceram. Soc.*, vol. 85, no. 5, pp. 1291–1293, Dec. 2004, doi: 10.1111/j.1151-2916.2002.tb00260.x.

[50] O. Popov and V. Vishnyakov, "Fracture toughness in some hetero-modulus composite carbides: carbon inclusions and voids," *Adv. Appl. Ceram.*, vol. 116, no. 2, pp. 61–70, Feb. 2017, doi: 10.1080/17436753.2016.1208470.

[51] D. Jianxin, "Erosion wear of boron carbide ceramic nozzles by abrasive air-jets," *Mater. Sci. Eng. A*, vol. 408, no. 1–2, pp. 227–233, 2005, doi: 10.1016/j.msea.2005.07.029.

[52] C. Cheng, K. M. Reddy, A. Hirata, T. Fujita, and M. Chen, "Structure and mechanical properties of boron-rich boron carbides," *J. Eur. Ceram. Soc.*, vol. 37, no. 15, pp. 4514–4523, 2017, doi: 10.1016/j.jeurceramsoc.2017.06.017.

[53] S. Wang, Y. Li, X. Xing, and X. Jing, "Low-temperature synthesis of high-purity boron carbide via an aromatic polymer precursor," *J. Mater. Res.*, vol. 33, no. 11, pp. 1659–1670, Jun. 2018, doi: 10.1557/jmr.2018.97.

[54] N. N. Greenwood, R. V. Parish, and P. Thornton, "87. Some reactions of metal borides," *J. Chem. Soc.*, p. 545, 1965, doi: 10.1039/jr9650000545.

[55] S. Shang, T. Wang, and Z. Liu, "Thermodynamic modelling of the B–Ca, B–Sr and B–Ba systems," *Calphad*, vol. 31, no. 2, pp. 286–291, Jun. 2007, doi: 10.1016/j.calphad.2006.11.005.

[56] O. Orhan, "Yerli Ham Bor Cevherinden Kalsiyum Hekzaborür Üretimi Ve Refrakterlerde Antioksidan Olarak Kullanilmasi," Istanbul Teknik Üniversitesi, 2006.

[57] H. Okamoto, "B-Ca (Boron-Calcium)," *J. Phase Equilibria Diffus.*, vol. 29, no. 4, pp. 379–379, Aug. 2008, doi: 10.1007/s11669-008-9301-4.

[58] B. J. Mean, K. H. Lee, K. H. Kang, M. Lee, J. S. Rhee, and B. K. Cho, "11B NMR study of calcium-hexaborides," *Phys. B Condens. Matter*, vol. 359–361, pp. 1204–1206, Apr. 2005, doi: 10.1016/j.physb.2005.01.346.

[59] Ö. Yildiz, R. Telle, C. Schmalzried, and A. Kaiser, "Phase transformation of transient B4C to CaB6 during production of CaB6 from colemanite," *J. Eur.*

Ceram. Soc., vol. 25, no. 14, pp. 3375–3381, Sep. 2005, doi: 10.1016/j.jeurceramsoc.2004.09.001.

[60] D. Yılmaz, "Boro/Karbotermik İndirgeme Yöntemiyle CaB6 Sentezi ve Karakterizasyonu," Eskişehir Osmangazi Üniversitesi, 2018.

[61] W. Reitz, "Ceramic Processing and Sintering by M. N. Rahaman," *Mater. Manuf. Process.*, vol. 12, no. 3, pp. 555–556, May 1997, doi: 10.1080/10426919708935164.

[62] S.-J. L. Kang, *Sintering*. Elsevier, 2005.

[63] A. Aytimur, S. Koçyiğit, and İ. Uslu, "Calcia Stabilized Ceria Doped Zirconia Nanocrystalline Ceramic," *J. Inorg. Organomet. Polym. Mater.*, vol. 24, no. 6, pp. 927–932, 2014, doi: 10.1007/s10904-014-0064-6.

[64] S. Kumar, "Selective Laser Sintering/Melting," in *Comprehensive Materials Processing*, vol. 10, Elsevier, 2014, pp. 93–134.

[65] R. M. German, "Thermodynamics of sintering," in Sintering of Advanced Materials, Elsevier, 2010, pp. 3–32.

[66] L. B. Kong *et al.*, *Transparent Ceramics*, no. I. Cham: Springer International Publishing, 2015.

[67] R. M. German, P. Suri, and S. J. Park, "Review: liquid phase sintering," *J. Mater. Sci.*, vol. 44, no. 1, pp. 1–39, Jan. 2009, doi: 10.1007/s10853-008-3008-0.

[68] R. M. German, *Liquid Phase Sintering*. Boston, MA: Springer US, 1985.

[69] D. Goll, R. Loeffler, D. Hohs, and G. Schneider, "Reaction sintering as a high-throughput approach for magnetic materials development," *Scr. Mater.*, vol. 146, pp. 355–361, Mar. 2018, doi: 10.1016/j.scriptamat.2017.05.004.

[70] J. K. Sonber, T. S. R. Ch. Murthy, C. Subramanian, R. C. Hubli, and A. K. Suri, "Processing Methods for Ultra High Temperature Ceramics," in *MAX Phases and Ultra-High Temperature Ceramics for Extreme Environments*, no. June 2016, IGI Global, 2013, pp. 180–202.

[71] L. A. Dobrzanski, A. D. Dobrzanska-Danikiewicz, A. Achtelik-Franczak, L. B. Dobrzanski, E. Hajduczek, and G. Matula, "Fabrication Technologies of the Sintered Materials Including Materials for Medical and Dental Application," in *Powder Metallurgy - Fundamentals and Case Studies*, InTech, 2017.

[72] R. S. Dobedoe, G. D. West, and M. H. Lewis, "Spark plasma sintering of ceramics: understanding temperature distribution enables more realistic comparison with conventional processing," *Adv. Appl. Ceram.*, vol. 104, no. 3, pp. 110–116, Jun. 2005, doi: 10.1179/174367605X16662.

[73] P. Cavaliere, *Spark plasma sintering of materials: Advances in processing and applications*. 2019.

[74] U. Akkaşoğlu, "HETEROJEN İÇYAPIYA SAHİP SERAMİK KESİCİ UÇLARIN GELİŞTİRİLMESİ," Anadolu Üniversitesi, 2018.

[75] M. Suarez *et al.*, "Challenges and Opportunities for Spark Plasma Sintering: A Key Technology for a New Generation of Materials," in *Sintering Applications*,

InTech, 2013.

[76] P. Boch and J.-C. Niepce, *Ceramic Materials: Processes, Properties, and Applications*. 2010.

[77] C. Barry Carter and M. Grant Norton, *Ceramic materials: Science and engineering*. 2007.

[78] G. I. Kalandadze, S. O. Shalamberidze, and A. B. Peikrishvili, "Sintering of Boron and Boron Carbide," *J. Solid State Chem.*, vol. 154, no. 1, pp. 194–198, Oct. 2000, doi: 10.1006/jssc.2000.8835.

[79] T. K. Roy, C. Subramanian, and A. K. Suri, "Pressureless sintering of boron carbide," *Ceram. Int.*, vol. 32, no. 3, pp. 227–233, Jan. 2006, doi: 10.1016/j.ceramint.2005.02.008.

[80] M. Mashhadi, E. Taheri-Nassaj, and V. M. Sglavo, "Pressureless sintering of boron carbide," *Ceram. Int.*, vol. 36, no. 1, pp. 151–159, Jan. 2010, doi: 10.1016/j.ceramint.2009.07.034.

[81] R. Angers and M. Beauvy, "Hot-pressing of boron carbide," *Ceram. Int.*, vol. 10, no. 2, pp. 49–55, 1984, doi: 10.1016/0272-8842(84)90025-7.

[82] Y. Celik, "Bor Karbür'ün Spark Plazma Yöntemiyle Sinterlenmesi, Çeşitli Sinterleme Katkilarinin Sinterleme Ve Malzeme Özelliklerine Etkileri," Istanbul Teknik Üniversitesi, 2010.

[83] S. Yamada, K. Hirao, Y. Yamauchi, and S. Kanzaki, "Mechanical and electrical properties of B4C–CrB2 ceramics fabricated by liquid phase sintering," *Ceram. Int.*, vol. 29, no. 3, pp. 299–304, 2003, doi: 10.1016/S0272-8842(02)00120-7.

[84] H. Suzuki, T. Hase, and T. Maruyama, "Effect of Carbon on the Sintering of Boron Carbide," *J. Ceram. Assoc. Japan*, vol. 87, no. 1008, pp. 430–433, 1979, doi: 10.2109/jcersj1950.87.1008_430.

[85] K. A. Schwetz and W. Grellner, "The influence of carbon on the microstructure and mechanical properties of sintered boron carbide," *J. Less Common Met.*, vol. 82, pp. 37–47, Nov. 1981, doi: 10.1016/0022-5088(81)90195-8.

[86] A. Goldstein, Y. Geffen, and A. Goldenberg, "Boron Carbide-Zirconium Boride In Situ Composites by the Reactive Pressureless Sintering of Boron Carbide-Zirconia Mixtures," *J. Am. Ceram. Soc.*, vol. 84, no. 3, pp. 642–644, Mar. 2001, doi: 10.1111/j.1151-2916.2001.tb00714.x.

[87] S. Tuffé, J. Dubois, G. Fantozzi, and G. Barbier, "Densification, microstructure and mechanical properties of TiB2-B4C based composites," *Int. J. Refract. Met. Hard Mater.*, vol. 14, no. 5–6, pp. 305–310, Jan. 1996, doi: 10.1016/S0263-4368(96)00012-1.

[88] K. D. Behler, J. C. LaSalvia, E. R. Shanholtz, M. C. Golt, S. Walck, and K. A. Kuwelkar, "Effect of Al2O3 on the Densification and Microstructure of B4C," in *Advances in Ceramic Armor, Bioceramics, and Porous Materials: Ceramic Engineering and Science Proceedings Volume 37, Issue 4, XXXVII*, Jan. 2017, vol. 37, no. 4, pp. 21–30, doi: 10.1002/9781119321682.ch3.

[89] P. Sahani, S. K. Karak, B. Mishra, D. Chakravarty, and D. Chaira, "Effect of Al

addition on SiC–B4C cermet prepared by pressureless sintering and spark plasma sintering methods," *Int. J. Refract. Met. Hard Mater.*, vol. 57, pp. 31–41, Jun. 2016, doi: 10.1016/j.ijrmhm.2016.02.005.

[90] M. V. Swain, R. W. Cahn, P. Haasen, and E. J. Kramer, *Materials science and technology: a comprehensive treatment*. VCH, 1994.

[91] J. Deng, J. Zhou, Y. Feng, and Z. Ding, "Microstructure and mechanical properties of hot-pressed B4C/(W,Ti)C ceramic composites," *Ceram. Int.*, vol. 28, no. 4, pp. 425–430, Jan. 2002, doi: 10.1016/S0272-8842(01)00113-4.

[92] M. Cafri, H. Dilman, M. P. Dariel, and N. Frage, "Boron carbide/magnesium composites: Processing, microstructure and properties," *J. Eur. Ceram. Soc.*, vol. 32, no. 12, pp. 3477–3483, 2012, doi: 10.1016/j.jeurceramsoc.2012.04.007.

[93] Y. KANNO, K. KAWASE, and K. NAKANO, "Additive Effect on Sintering of Boron Carbide," *J. Ceram. Assoc. Japan*, vol. 95, no. 1107, pp. 1137–1140, 1987, doi: 10.2109/jcersj1950.95.1107_1137.

[94] X. Du, Y. Wang, Z. Zhang, F. Zhang, W. Wang, and Z. Fu, "Effects of silicon addition on the microstructure and properties of B4C–SiC composite prepared with polycarbosilane-coated B4C powder," *Mater. Sci. Eng. A*, vol. 636, pp. 133–137, Jun. 2015, doi: 10.1016/j.msea.2015.03.049.

[95] H. Miyazaki, Y. Zhou, H. Hyuga, Y. Yoshizawa, and T. Kumazawa, "Microstructure of boron carbide pressureless sintered in an Ar atmosphere containing gaseous metal species," *J. Eur. Ceram. Soc.*, vol. 30, no. 4, pp. 999–1005, Mar. 2010, doi: 10.1016/j.jeurceramsoc.2009.10.015.

[96] J. Sun, C. Liu, and R. Wang, "Low pressure hot pressing of B4C matrix ceramic composites improved by Al2O3 and TiC additives," *Mater. Sci. Eng. A*, vol. 519, no. 1–2, pp. 27–31, Aug. 2009, doi: 10.1016/j.msea.2009.06.016.

[97] H.-W. Kim, Y. Koh, and H. Kim, "Densification and Mechanical Properties of B4C with Al2O3 as a Sintering Aid," *J. Am. Ceram. Soc.*, vol. 83, no. 11, pp. 2863–2865, Dec. 2004, doi: 10.1111/j.1151-2916.2000.tb01647.x.

[98] Z. Yuhua, L. Aiju, Y. Yansheng, S. Ruixia, and L. Yingcai, "Reactive and dense sintering of reinforced-toughened B4C matrix composites," *Mater. Res. Bull.*, vol. 39, no. 11, pp. 1615–1625, Sep. 2004, doi: 10.1016/j.materresbull.2004.05.011.

[99] L. Levin, N. Frage, and M. . Dariel, "A novel approach for the preparation of B4C-based cermets," *Int. J. Refract. Met. Hard Mater.*, vol. 18, no. 2–3, pp. 131–135, Mar. 2000, doi: 10.1016/S0263-4368(00)00012-3.

[100] M. Kakazey, M. Vlasova, J. G. Gonzalez-Rodriguez, M. Dominguez-Patiño, and R. Leder, "X-ray and EPR study of reactions between B4C and TiO2," *Mater. Sci. Eng. A*, vol. 418, no. 1–2, pp. 111–114, Feb. 2006, doi: 10.1016/j.msea.2005.11.018.

[101] R. M. Da Rocha and F. C. Lourenço de Melo, "Effect of TiO2 and TiB2 on pressureless sintering of B4C," *Mater. Sci. Forum*, vol. 727–728, pp. 1022–

1027, 2012, doi: 10.4028/www.scientific.net/MSF.727-728.1022.

[102] J. E. Zorzi, C. A. Perottoni, and J. A. H. da Jornada, “Hardness and wear resistance of B4C ceramics prepared with several additives,” *Mater. Lett.*, vol. 59, no. 23, pp. 2932–2935, Oct. 2005, doi: 10.1016/j.matlet.2005.04.047.

[103] K. Miyazaki, T. Hagio, and K. Kobayashi, “Graphite and boron carbide composites made by hot-pressing,” *J. Mater. Sci.*, vol. 16, no. 3, pp. 752–762, Mar. 1981, doi: 10.1007/BF02402792.

[104] O. Popov and V. Vishnyakov, “Fracture toughness in some hetero-modulus composite carbides: carbon inclusions and voids,” *Adv. Appl. Ceram.*, vol. 116, no. 2, pp. 61–70, Feb. 2017, doi: 10.1080/17436753.2016.1208470.

[105] M. Asadikiya, C. Rudolf, C. Zhang, B. Boesl, and Y. Zhong, “The Role of Calphad Approach in the Sintering of B4C with SIC as a Sintering Aid by Spark Plasma Sintering Technique,” *Addit. Manuf. Strateg. Technol. Adv. Ceram.*, vol. 258, no. January, pp. 185–191, 2016, doi: 10.1002/9781119236016.ch19.

[106] Z. Zhang, X. Du, W. Wang, Z. Fu, and H. Wang, “Preparation of B4C–SiC composite ceramics through hot pressing assisted by mechanical alloying,” *Int. J. Refract. Met. Hard Mater.*, vol. 41, pp. 270–275, Nov. 2013, doi: 10.1016/j.ijrmhm.2013.04.012.

[107] H. Miyazaki, Y. Zhou, H. Hyuga, Y. Yoshizawa, and T. Kumazawa, “Microstructure of boron carbide pressureless sintered in an Ar atmosphere containing gaseous metal species,” *J. Eur. Ceram. Soc.*, vol. 30, no. 4, pp. 999–1005, Mar. 2010, doi: 10.1016/j.jeurceramsoc.2009.10.015.

[108] C. Xu, Y. Cai, K. Flodström, Z. Li, S. Esmaeilzadeh, and G. Zhang, “Spark plasma sintering of B4C ceramics: The effects of milling medium and TiB2 addition,” *Int. J. Refract. Met. Hard Mater.*, vol. 30, no. 1, pp. 139–144, Jan. 2012, doi: 10.1016/j.ijrmhm.2011.07.016.

[109] H. R. Baharvandi, A. M. Hadian, and A. Alizadeh, “Processing and mechanical properties of boron carbide-titanium diboride ceramic matrix composites,” *Appl. Compos. Mater.*, vol. 13, no. 3, pp. 191–198, 2006, doi: 10.1007/s10443-006-9012-0.

[110] Z. Liu, X. Deng, J. Li, Y. Sun, and S. Ran, “Effects of B4C particle size on the microstructures and mechanical properties of hot-pressed B4C–TiB2 composites,” *Ceram. Int.*, vol. 44, no. 17, pp. 21415–21420, Dec. 2018, doi: 10.1016/j.ceramint.2018.08.200.

[111] Q. He, A. Wang, C. Liu, W. Wang, H. Wang, and Z. Fu, “Microstructures and mechanical properties of B4C-TiB2-SiC composites fabricated by ball milling and hot pressing,” *J. Eur. Ceram. Soc.*, vol. 38, no. 7, pp. 2832–2840, Jul. 2018, doi: 10.1016/j.jeurceramsoc.2018.02.020.

[112] E. Ayas, A. Kalemtas, G. Arslan, A. Kara, and F. Kara, “Spark Plasma Sintering of Silicon Nitride-Boron Carbide Composites,” *Key Eng. Mater.*, vol. 403, pp. 225–226, 2008, doi: 10.4028/www.scientific.net/kem.403.225.

[113] E. Ayas, A. Kalemtas, G. Arslan, A. Kara, and F. Kara, “Spark plasma sintering of

Si3N4-B4C composites," *J. Ceram. Soc. Japan*, vol. 116, no. 1354, pp. 727–731, 2008, doi: 10.2109/jcersj2.116.727.

[114] T. Jiang, Z. H. Jin, J. F. Yang, and G. J. Qiao, "High Temperature Oxidation Behavior of the B4C/BN Composites," *Adv. Mater. Res.*, vol. 105–106, pp. 133–136, Apr. 2010, doi: 10.4028/www.scientific.net/AMR.105-106.133.

[115] O. N. Grigor'ev *et al.*, "Sintered ceramics based on boron nitride and carbide," *Powder Metall. Met. Ceram.*, vol. 46, no. 1–2, pp. 46–50, Jan. 2007, doi: 10.1007/s11106-007-0009-5.

[116] M. da R. Rosa and C. L. de M. Francisco, "Sintering of B4C-SiC composites with ALN-Y2O3 addition," *Mater. Sci. Forum*, vol. 727–728, pp. 850–855, 2012, doi: 10.4028/www.scientific.net/MSF.727-728.850.

[117] M. Çirakoğlu, Ç. Toy, A. Tekin, and W. D. Scott, "The formation of aluminium nitride-boron carbide-aluminium composites by wetting assisted infiltration," *Ceram. Int.*, vol. 23, no. 2, pp. 115–118, 1997, doi: 10.1016/s0272-8842(96)00005-3.

[118] D. I. Yushin, A. V Smirnov, P. Y. Peretyagin, and R. Torrecillas, "Mechanics Industry Cutting tools: finite element modeling of spark plasma sintering to improve their quality," vol. 713, 2015, doi: 10.1051/meca/2015.

PUBLICATIONS FROM THE THESIS

Contact Information: yasinbozkurtyilmaz@hotmail.com

Conference Papers

1. Y. Yılmaz, U. Akkaşoğlu and B. Çiçek, "Low Temperature Densification of B4C Ceramics with CaB6 Additives", in The 7th International Scientific Research Congress – Science and Engineering, Ankara/Turkey, 2020.